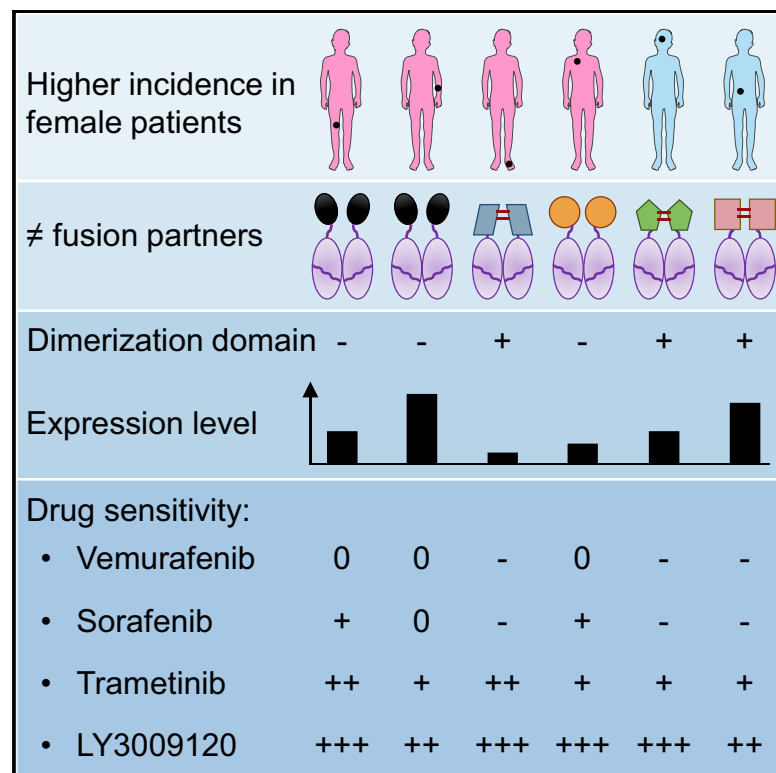


Genetic Heterogeneity of BRAF Fusion Kinases in Melanoma Affects Drug Responses

Graphical Abstract



Authors

Thomas Botton, Eric Talevich, Vivek Kumar Mishra, ..., Nicholas K. Hayward, Iwei Yeh, Boris C. Bastian

Correspondence

thomas.botton@unice.fr (T.B.), boris.bastian@ucsf.edu (B.C.B.)

In Brief

Botton et al. shed light on the heterogeneity of BRAF fusions encountered in melanocytic tumors and characterize features influencing their signaling and drug response. These findings unveil the singularities of BRAF fusions and establish general principles to guide their clinical management in melanoma and other malignancies.

Highlights

- BRAF fusions of melanocytic tumors are associated with younger age and female gender
- Numerous fusion partners exist with variations in signaling and drug response
- Fusion partners alter drug responses via dimerization and expression levels
- Next-generation RAF inhibitors are most effective and synergize with MEK inhibitors



Genetic Heterogeneity of BRAF Fusion Kinases in Melanoma Affects Drug Responses

Thomas Botton,^{1,2,3,9,*} Eric Talevich,^{1,2,3} Vivek Kumar Mishra,^{1,2,3} Tongwu Zhang,⁴ A. Hunter Shain,^{1,2,3} Céline Berquet,^{1,2,3} Alexander Gagnon,^{1,2,3} Robert L. Judson,^{1,2} Robert Ballotti,⁵ Antoni Ribas,⁶ Meenhard Herlyn,⁷ Stéphane Rocchi,⁵ Kevin M. Brown,⁴ Nicholas K. Hayward,⁸ Iwei Yeh,^{1,2,3} and Boris C. Bastian^{1,2,3,10,*}

¹Helen Diller Family Comprehensive Cancer Center, University of California, San Francisco, San Francisco, CA 94158, USA

²Department of Dermatology, University of California, San Francisco, San Francisco, CA 94115, USA

³Department of Pathology, University of California, San Francisco, San Francisco, CA 94115, USA

⁴Laboratory of Translational Genomics, Division of Cancer Epidemiology and Genetics, National Cancer Institute, NIH, Bethesda, MA 20892, USA

⁵U1065, Institut National de la Santé et de la Recherche Médicale, Centre Méditerranéen de Médecine Moléculaire, Université Côte d'Azur, 06200 Nice, France

⁶Jonsson Comprehensive Cancer Center, University of California, Los Angeles, Los Angeles, CA 90095, USA

⁷Molecular and Cellular Oncogenesis Program and Melanoma Research Center, The Wistar Institute, Philadelphia, PA 19104, USA

⁸Oncogenomics Laboratory, QIMR Berghofer Medical Research Institute, Brisbane, QLD 4006, Australia

⁹Present address: U1065, Institut National de la Santé et de la Recherche Médicale, Centre Méditerranéen de Médecine Moléculaire, Université Côte d'Azur, 06200 Nice, France

¹⁰Lead Contact

*Correspondence: thomas.botton@unice.fr (T.B.), boris.bastian@ucsf.edu (B.C.B.)

<https://doi.org/10.1016/j.celrep.2019.09.009>

SUMMARY

BRAF fusions are detected in numerous neoplasms, but their clinical management remains unresolved. We identified six melanoma lines harboring BRAF fusions representative of the clinical cases reported in the literature. Their unexpected heterogeneous responses to RAF and MEK inhibitors could be categorized upon specific features of the fusion kinases. Higher expression level correlated with resistance, and fusion partners containing a dimerization domain promoted paradoxical activation of the mitogen-activated protein kinase (MAPK) pathway and hyperproliferation in response to first- and second-generation RAF inhibitors. By contrast, next-generation α C-IN/DFG-OUT RAF inhibitors blunted paradoxical activation across all lines and had their therapeutic efficacy further increased *in vitro* and *in vivo* by combination with MEK inhibitors, opening perspectives in the clinical management of tumors harboring BRAF fusions.

INTRODUCTION

Oncogenic BRAF fusions originate from genomic rearrangements placing the 3' portion of the *BRAF* gene encoding the kinase domain behind another gene at the 5' position. The rearrangements result in the expression of oncoproteins that are constitutively active due to loss of the auto-inhibitory domain of BRAF and whose expression is controlled by the promoter of the 5' partner (Lu et al., 2017).

BRAF fusions are among the most common kinase translocations in solid tumors (Stransky et al., 2014; Yoshihara et al., 2015; Zehir et al., 2017). Since their first description in 2005 as bona fide oncogenes in papillary thyroid carcinoma (Ciampi et al., 2005), hundreds of tumors in which the BRAF kinase domain is fused to one of more than 110 different partner genes have been identified spanning 15 different tumor types (COSMIC, <https://cancer.sanger.ac.uk/cosmic/gene/analysis?in=BRAF>) (Ross et al., 2016; Zehir et al., 2017). As the genomic breakpoints usually reside within introns of the two fusion partners, they are typically not detected by exome sequencing. Thus, the number of common and rare cancer types with recurrent BRAF fusions is likely to increase as more comprehensive genomic analyses are performed.

BRAF fusions are particularly common in pilocytic astrocytoma (Cin et al., 2011; Jones et al., 2008, 2013) and pancreatic acinar cell carcinoma (Chmielecki et al., 2014; Ross et al., 2016). In unselected melanomas, BRAF fusions are estimated to occur in 2.6%–6.7% of cases (Table S1), but their frequency is higher in certain histopathologic subtypes (Botton et al., 2013; Ross et al., 2016; Wiesner et al., 2014). Moreover, recent reports described the emergence of BRAF fusions as a resistance mechanism in EGFR mutant lung cancers treated with tyrosine kinase inhibitors (Schrock et al., 2018; Yu et al., 2018), in gastric cancer treated with FGFR inhibitors (Sase et al., 2018), and in BRAF^{V600E} mutant melanomas treated with vemurafenib (Kulkarni et al., 2017).

How to therapeutically target tumors driven by BRAF fusions therefore is an increasingly important question. Currently, the clinical experience consists of case studies with partially conflicting results. For instance, while sorafenib-based treatment of low-grade astrocytomas harboring KIAA1549-BRAF fusions can result in accelerated tumor growth (Karajannis et al., 2014), case reports of a spindle cell neoplasm harboring an identical



fusion (Subbiah et al., 2014) and a melanoma harboring an AGK-BRAF fusion (Botton et al., 2013; Passeron et al., 2011) showed clinically meaningful responses.

Several *in vitro* studies have been carried out to demonstrate the transforming activity of various *BRAF* fusion genes. It was established that ectopically expressed *BRAF* fusion proteins signal by dimerization in a RAS-independent manner (Kim et al., 2017; Sievert et al., 2013; Yao et al., 2015). However, limited information is available on the drug sensitivity of *BRAF* fusion kinases, in part because of the scarcity of cell lines carrying these alterations (Kim et al., 2017; Turner et al., 2019). Most studies were therefore restricted to the use of engineered models, in which the cellular expression level of the fusion kinases and the genetic context are expected to be different from the ones found in cancers driven by *BRAF* fusions (Chakraborty et al., 2016; Chmielecki et al., 2014; Diamond et al., 2016; Hutchinson et al., 2013; Lu et al., 2017; Olow et al., 2016; Palanisamy et al., 2010; Sievert et al., 2013). The identification of *BRAF* fusions in already established cell lines or the generation of cell lines from tumors with *BRAF* fusions could address this critical bottleneck. Despite extensive efforts in studying pilocytic astrocytoma, patient-derived xenografts and unmodified cell lines harboring KIAA1549-*BRAF* fusions have failed to establish (Selt et al., 2017).

RESULTS

In Melanocytic Tumors, BRAF Fusions Are Associated with Female Sex and Show a Wide Range of 3' Partners

We performed a systematic review of the literature of *BRAF* fusions found in melanocytic tumors and identified 100 reported cases. In contrast to other cancer types, *BRAF* fusions are more prevalent in female patients with melanocytic tumors (two-tailed p value from binomial test is 0.0004; Figure 1A; Tables S2 and S3). The spectrum of reported cases reaches from benign nevi to melanoma that metastasized, indicating that *BRAF* fusions are early driver events (Figure 1B), and are often associated with spitzoid histopathologic features (Figure 1C). Melanocytic neoplasms with *BRAF* fusions arose anywhere on the skin and mucosa, without preference for a specific anatomic site (Figure 1D). Overall, melanocytic tumors in young patients appear to be enriched for *BRAF* fusions (Figure 1E), with a mean age at presentation of 33 years (range, 0–79). When considering only melanomas with *BRAF* fusions, the median age was 39 years (range, 1–79; Table S4) compared to 63 years for all cutaneous melanomas according to the American Cancer Society.

While all *BRAF* fusion genes detected in melanocytic tumors preserved the portion encoding the *BRAF* kinase domain, the location of the breakpoints occurred in introns 7–10 (Figure 1F), with intron 8 being the most common location. There was no difference in the distribution of breakpoints between benign and malignant tumors (Table S4). In contrast to pilocytic astrocytoma that are characterized by highly recurrent KIAA1549-*BRAF* fusions (Jones et al., 2013), 42 different 5' partners have been reported for *BRAF* fusions in melanocytic tumors (Figure 1G). Of these, only eight 5' partners were recurrent, with AGK and AKAP9 as the most common partner gene (eight cases each). *BRAF* fusions dimerize via their RAF dimer interface to signal

(Sievert et al., 2013), but only 55% of reported *BRAF* fusion partners contributed additional dimerization domains suggesting that they may not be essential for transformation. There was no apparent difference in the distribution of fusion partners and presence or absence of a dimerization domain in the 5' partner between benign and malignant tumors (Table S4).

Identification of BRAF Fusions in Melanoma Cell Lines

We used targeted DNA sequencing (see STAR Methods for details) to screen 14 patient-derived melanoma cell lines known to lack oncogenic mutations in *BRAF* or *NRAS* to identify cell lines harboring *BRAF* fusions. Alterations in known melanoma drivers such as *NF1*, *KRAS*, *RAF1*, *KIT*, *NRAS*, or *CCND1* were identified in eight cell lines (Figure 2A; Table S6). Five of the remaining six cell lines showed chimeric reads that mapped to introns of *BRAF* indicating the presence of *BRAF* fusions that were confirmed by RNA sequencing. RNA sequencing of the sixth cell line revealed a *BRAF* fusion that was missed by DNA sequencing. All six cell lines with *BRAF* fusions lacked mutations in other melanoma oncogenes known to activate the mitogen-activated protein kinase (MAPK) signaling pathway. Cell lines with *BRAF* fusions had low to intermediate mutation burden similar to melanoma cell lines without *BRAF* fusions (Figure S2).

DNA and RNA analyses gave partially discrepant results. DNA sequence failed to correctly predict the fusion transcript and misidentified the fusion partner in three of the five cases, where a breakpoint in a *BRAF* intron was identified (Table S5). The apparent discrepancy between DNA sequencing (DNA-seq) and RNA sequencing (RNA-seq) results is likely due to the presence of complex rearrangements as observed in the SK-MEL-23 cell line presenting multiple breakpoints that makes it difficult or impossible to predict the 5' partner gene to *BRAF* from short reads of DNA (Figure S1). The fact that the *SKAP2-BRAF* fusion in the WM3928 cell line was missed by targeted DNA sequencing was likely due to uneven coverage over the intronic DNA sequencing, highlighting the limitations of DNA sequencing for fusion detection.

The presence of *BRAF* fusions was confirmed by western blot analysis using antibodies directed against the C-terminal part of *BRAF* and against p-*BRAF* S445. Aberrant bands, uniquely present in the six cell lines with *BRAF* fusions, were observed at the molecular weight matching the fusions products predicted from the RNA sequencing data (Figures 2B and S2C; Tables S5 and S7). Transfection of the cell lines harboring *BRAF* fusions with a pool of small interfering RNA (siRNA) targeting the C-terminal-encoding portion of the *BRAF* gene led to marked decrease in cell viability, indicating “oncogene addiction” to the fusions (Figure S2C).

All cell lines with *BRAF* fusions showed activation levels of the MAPK signaling pathway comparable to melanoma cell lines with *BRAF*^{V600E} mutations, which—in the absence of other mutations in the MAPK pathway—indicates that *BRAF* fusion kinases are functional. Consistent with Figure 1G depicting the broad spectrum of *BRAF* fusions in melanocytic tumors, diverse fusion kinases were identified in the cell lines, with AGK-*BRAF* fusion as the only recurrent fusion. Only two fusion partners were predicted to contribute additional dimerization domain to the fusion protein (Figure 2C). Thus, our small cohort of cell lines is

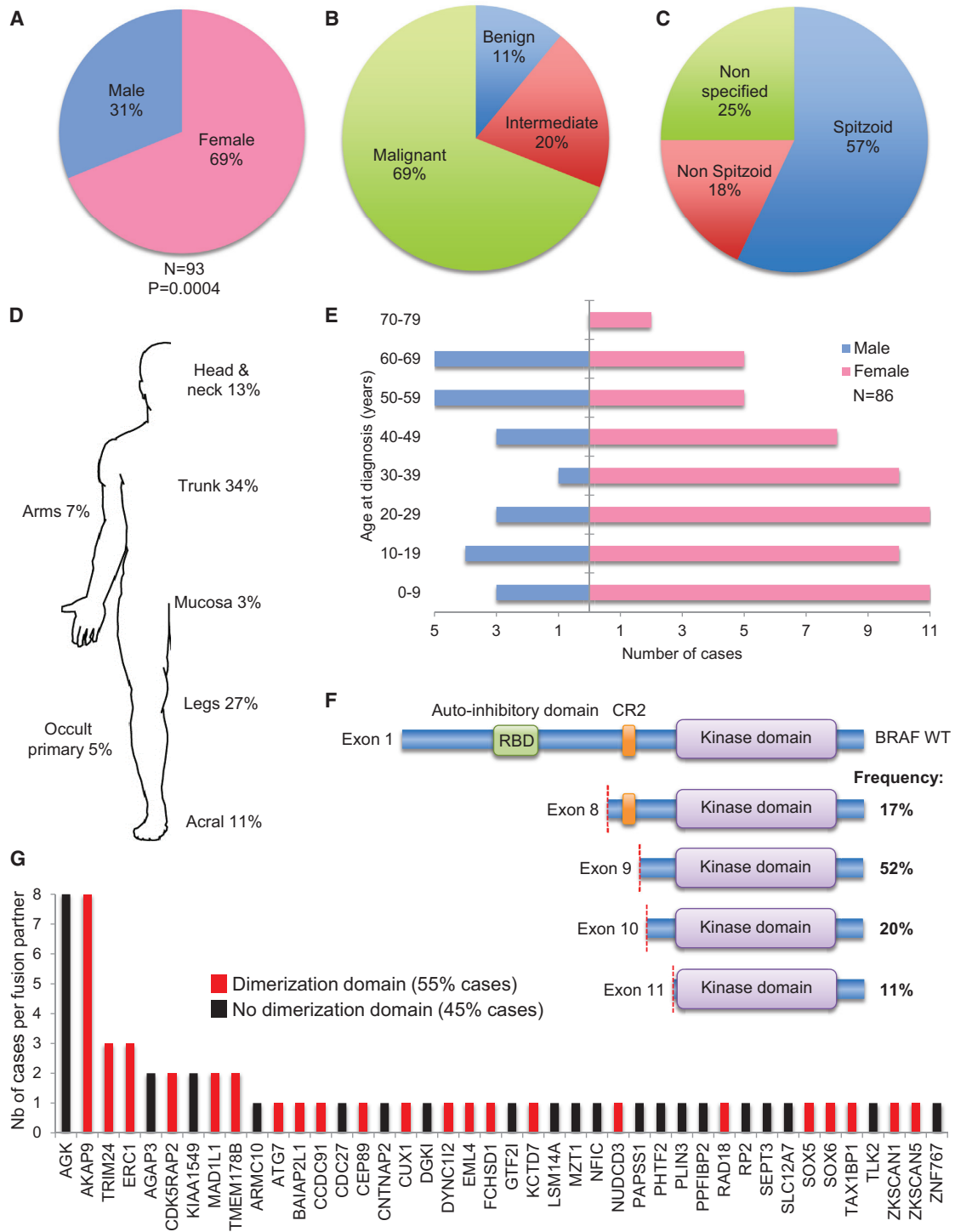


Figure 1. Clinical, Histologic, and Genetic Features of Published Melanocytic Tumors Harboring BRAF Fusions

(A–G) Distribution of sex (A; N = 93), tumor stage (B; N = 100), histology (C; N = 100), anatomic site (D; N = 67), age (E; N = 86), breakpoints within BRAF (F; N = 65), and 5' partners with (red) and without (black) dimerization domains (G; N = 65).

See also Tables S1, S2, and S3.

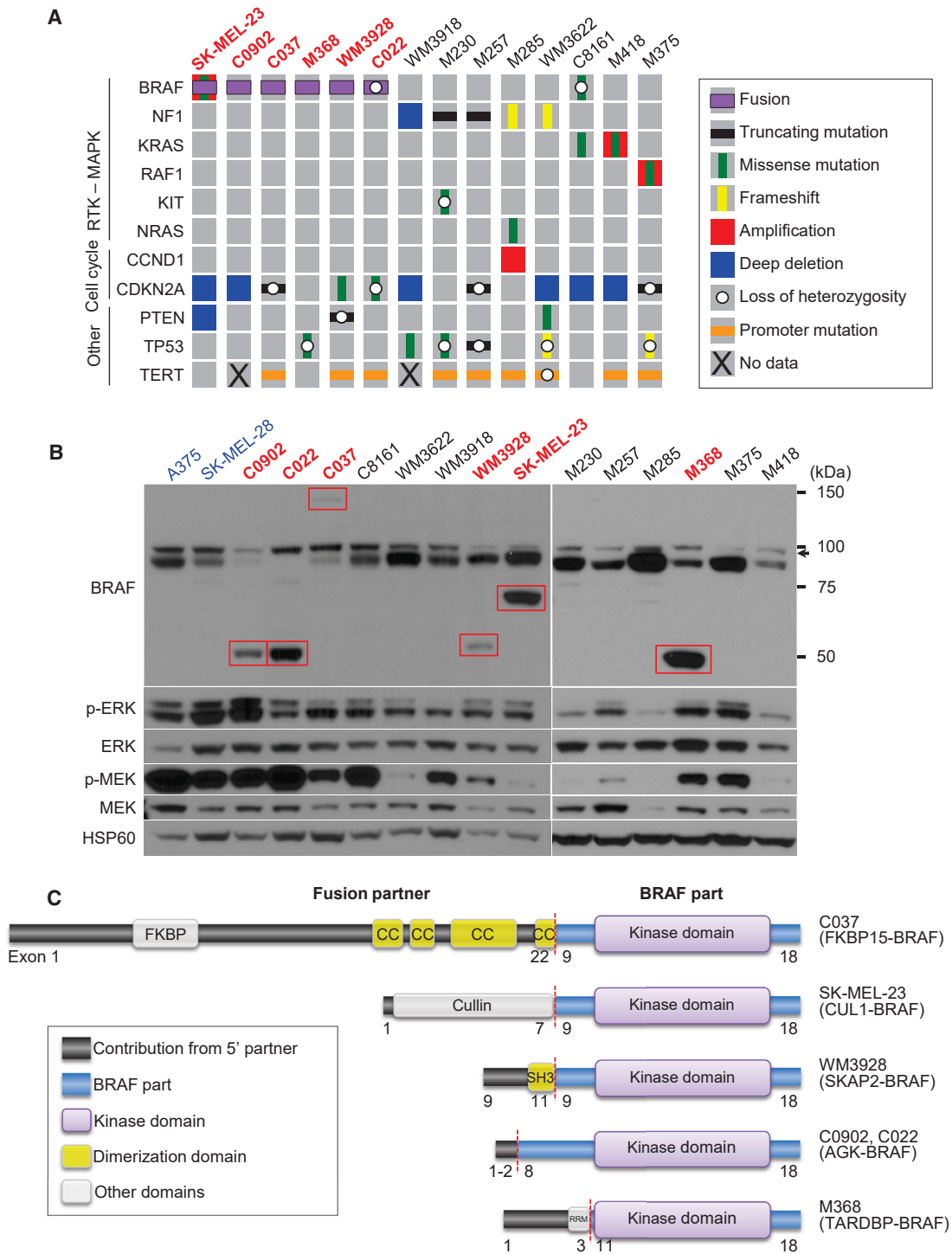


Figure 2. Identification of Six Melanoma Cell Lines Harboring BRAF Fusions

(A) Tiling plot of oncogenic drivers (rows) in 14 “pan-negative” melanoma cell lines (columns).

(B) Western blots of the 14 cell lines and two control BRAF^{V600E} mutant cell lines (A375 and SK-MEL-28). Red labels highlight cell lines in which sequencing identified *BRAF* fusions, with the corresponding fusion proteins at their predicted molecular weight (red boxes). The arrow indicates non-specific band at approximately 90 kDa detected by the BRAF antibody.

(C) Structural details of the identified fusions showing the contribution from the 5' partner in dark gray and BRAF in blue. Relevant protein domains identified by InterPro are superimposed as described in the figure legend.

See also [Figures S1](#) and [S2](#) and [Tables S4](#), [S5](#), [S6](#), and [S7](#).

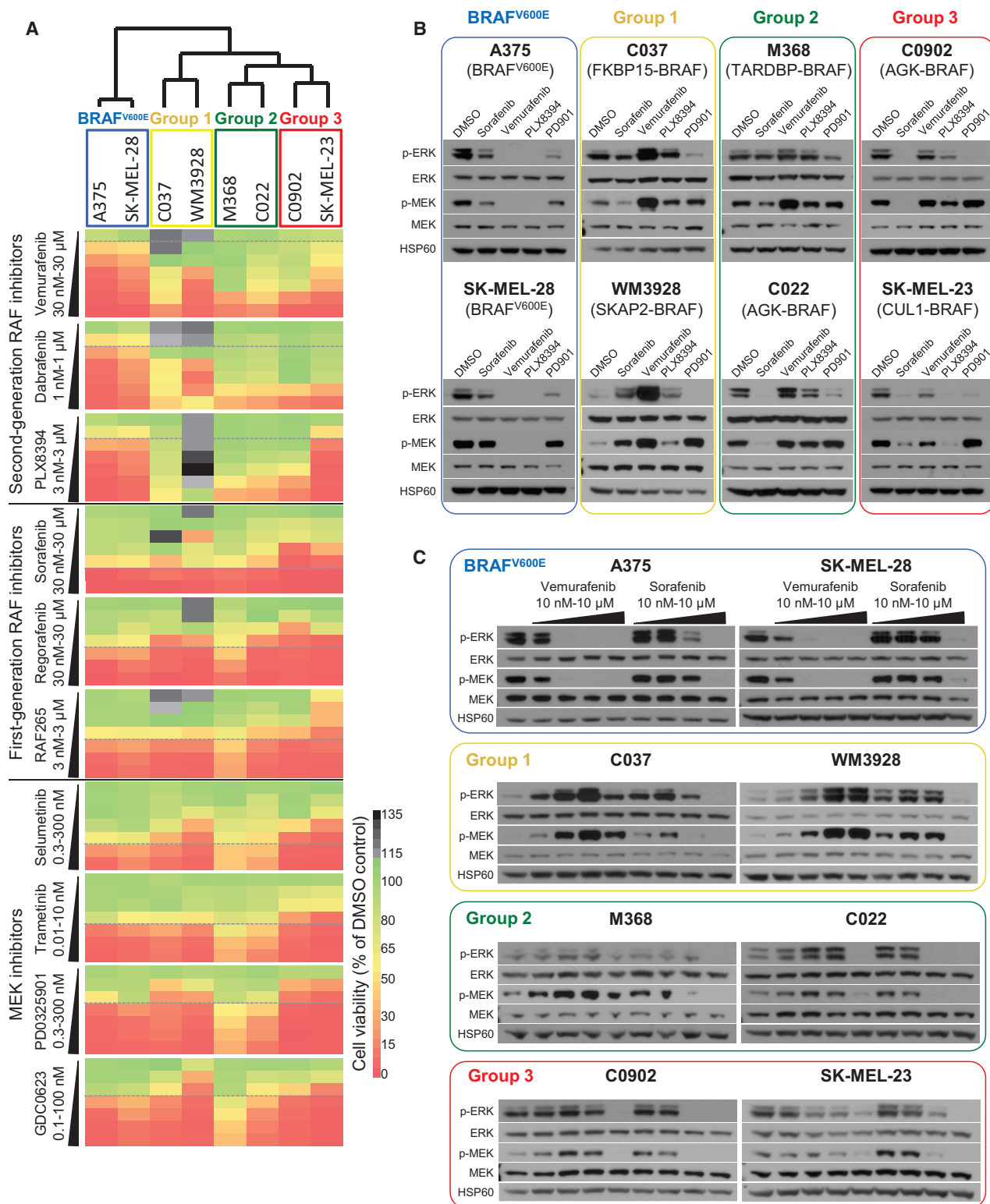


Figure 3. Heterogeneous Patterns of Drug Response to RAF and MEK Inhibitors of Cell Lines Harboring BRAF Fusions Compared to BRAF^{V600E} Mutant Lines

(A) Heatmap with cell viability after 5 days of treatment with RAF inhibitors of first and second generation or MEK inhibitors compared to DMSO-treated cells. The dotted gray lines indicate absolute IC₅₀ values in BRAF^{V600E} mutant cell lines for comparison. Cell lines were ordered horizontally by unsupervised hierarchical clustering. Data represent the average of three independent experiments with technical triplicates.

(legend continued on next page)

representative of BRAF fusions found in melanocytic tumors (Table S4).

Melanoma Cell Lines with BRAF Fusions Show Heterogeneous Responses to MEK and RAF Inhibitors

We assessed the sensitivity profile of the six cell lines with BRAF fusions to a panel of clinically used RAF and MEK inhibitors at dose levels known to be relevant in patients and benchmarked responses to two commonly used BRAF^{V600E} mutant melanoma lines.

We observed a wide range of drug responses across the different cell lines harboring BRAF fusions (Figure 3A) ranging from growth inhibition and/or cell death in some lines to increased proliferation in others, generally accompanied by corresponding pharmacodynamic effects on the MAPK signaling pathway (Figure 3B). To help the interpretation of the results, unsupervised clustering of the drug responses was performed and yielded three distinct groups. C037 and WM3928 cell lines (group 1) were characterized by increased proliferation at low doses of first- and second-generation RAF inhibitors, with concomitant paradoxical activation of the MAPK signaling pathway that waned at higher drug concentrations (Figures 3A and 3C). A second group composed of M368 and C022 was characterized by resistance to RAF and MEK inhibitors with modest inhibitory effects on proliferation and MAPK pathway. Group 3, composed of C0902 and SK-MEL-23, was sensitive to MEK and first-generation RAF inhibitors. Notably, all tested cell lines carrying BRAF fusions were resistant to vemurafenib and dabrafenib, sharply distinguishing them from BRAF^{V600E} mutant cell lines. Cell lines with BRAF fusions, except SK-MEL-23, demonstrated resistance to PLX8394, a BRAF inhibitor developed as a “paradox breaker.” Unexpectedly, treatment of the WM3928 cell line with PLX8394 resulted in paradoxical activation of the MAPK signaling pathway and increased proliferation (Figures 3A, 3B, and S3C).

As previously discussed, BRAF fusion genes differ in the position of the breakpoints within BRAF, which can occur in introns 7, 8, 9, or 10. Additional complexity is added by their respective 5' partner genes, which contribute different amino acid sequences that result in distinct functional domains and may or may not harbor domains that promote dimerization. The 5' partner genes can potentially further affect biological responses as their promoters control the expression level of the fusion kinases. Additionally, different BRAF fusion kinases may have variable stability and subcellular localization.

Our results suggest that the presence of portions of BRAF upstream of the kinase domain did not affect drug sensitivity, as the fusion junctions occurred in intron 7 in cell lines from groups 2 and 3, or intron 8 in cell lines from groups 1 and 3 (Figures 2C and 3A). Similarly, neither subcellular localization of BRAF fusion proteins analyzed by cell fractionation assays (Figure S3A) nor their stability monitored by cycloheximide treatment (Figure S3B) seem to correlate with drug sensitivity.

Higher Expression Level of BRAF Fusion Kinase Promotes Drug Resistance

We next sought to investigate why the cell lines in group 2 were generally more resistant to mitogen-activated protein kinase (MAPK) inhibitors than their counterparts in group 3. Notably the C022 and C0902 cell lines clustered differently (group 2 versus 3), although they harbored the exact same AGK-BRAF fusion. Globally, the C022 cell line showed a higher level of resistance to the tested drugs than C0902 (Figure 4A). However, the C022 line showed higher expression levels of the fusion protein than C0902, likely resulting from loss of the wild-type BRAF gene and copy number increase of the fusion gene (Figures 4B and S4), which could explain the differences in drug response. Increased gene dosage of a mutant BRAF^{V600E} allele also causes increased oncoprotein expression resulting in relative resistance to BRAF and MEK inhibition (Kemper et al., 2015; Moriceau et al., 2015). We transduced increasing amounts of AGK-BRAF fusion into 293FT cells and found that higher expression levels of the fusion protein blunted the inhibitory effect even of high concentrations of the RAF inhibitor sorafenib (Figure 4C) and MEK inhibitor selumetinib (Figure 4D) on the MAPK signaling pathway. Similarly, the overexpression of the AGK-BRAF fusion kinase in the C0902 cell line resulted in an increase of basal MAPK signaling and made the cells more resistant to sorafenib and trametinib (Figures 4E and 4F).

A relationship between the expression level of the fusion protein and drug resistance was further supported by the observation that the M368 cell line, which demonstrated marked resistance to most tested drugs presented, had the highest expression level of fusion protein of all cell lines (Figure 4G).

Dimerization Domains in the 5' Partner Cause RAS-Independent Paradoxical MAPK Activation in Response to First- and Second-Generation RAF Inhibitors

The C037 and WM3928 cell lines stood out through strong paradoxical activation of the MAPK signaling pathway and overproliferation upon first- and second-generation RAF inhibitor treatment. Their BRAF fusion proteins differ from other cell lines by a dimerization domain contributed by their 5' partners. To evaluate the role of these additional dimerization domains in RAF inhibitor-mediated paradoxical activation, we expressed BRAF fusions with and without dimerization domains in two different isogenic cellular models, immortalized mouse melanocytes (melan-a cells) and 293FT cells. When we expressed an AGK-BRAF fusion protein, which lacks dimerization domains contributed by the 5' partner, in melan-a cells we observed no paradoxical activation in response to RAF inhibitors. By contrast, when we expressed the ZKSCAN5-BRAF fusion protein that contains a SCAN dimerization domain, we observed marked paradoxical activation (Figure 5A). Corresponding results were obtained in 293FT cells, in which we expressed the NUDCD3-BRAF fusion protein harboring a coiled-coil domain finding paradoxical activation upon inhibitor treatment, whereas the

(B) Western blot analysis from serum-starved cells treated for 1 h with DMSO, 1 μ M sorafenib, 1 μ M vemurafenib, 100 nM PLX8394, or 1 nM PD0325901 (PD901). (C) Strong dose-dependent paradoxical activation of the MAPK pathway in serum-starved cell lines from group 1 upon treatment with vemurafenib or sorafenib (0, 0.01, 0.1, 1, or 10 μ M) for 1 h.

See also Figure 3.

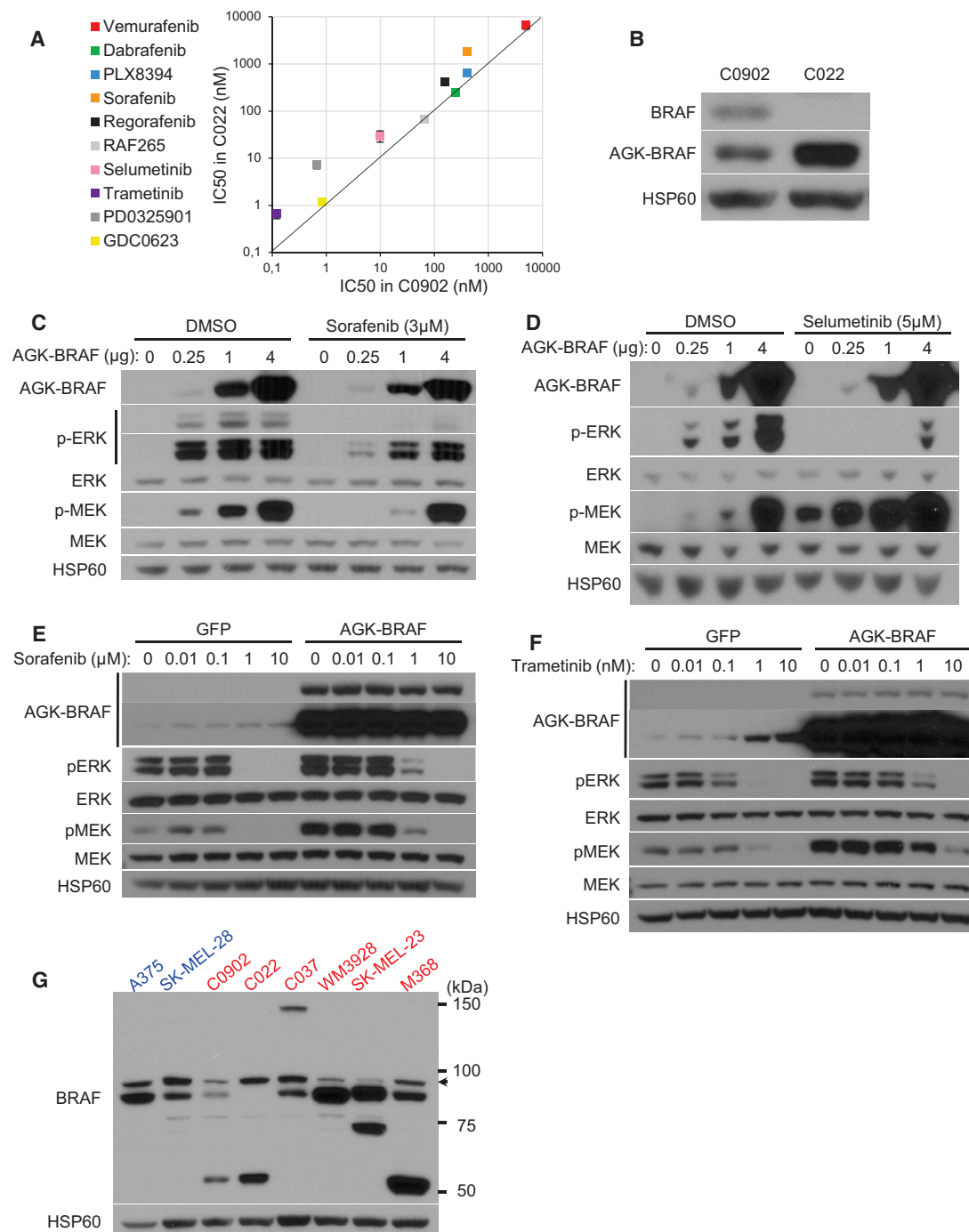


Figure 4. Increasing Expression Levels of BRAF Fusions Proteins Decrease the Effectiveness of RAF and MEK Inhibitors

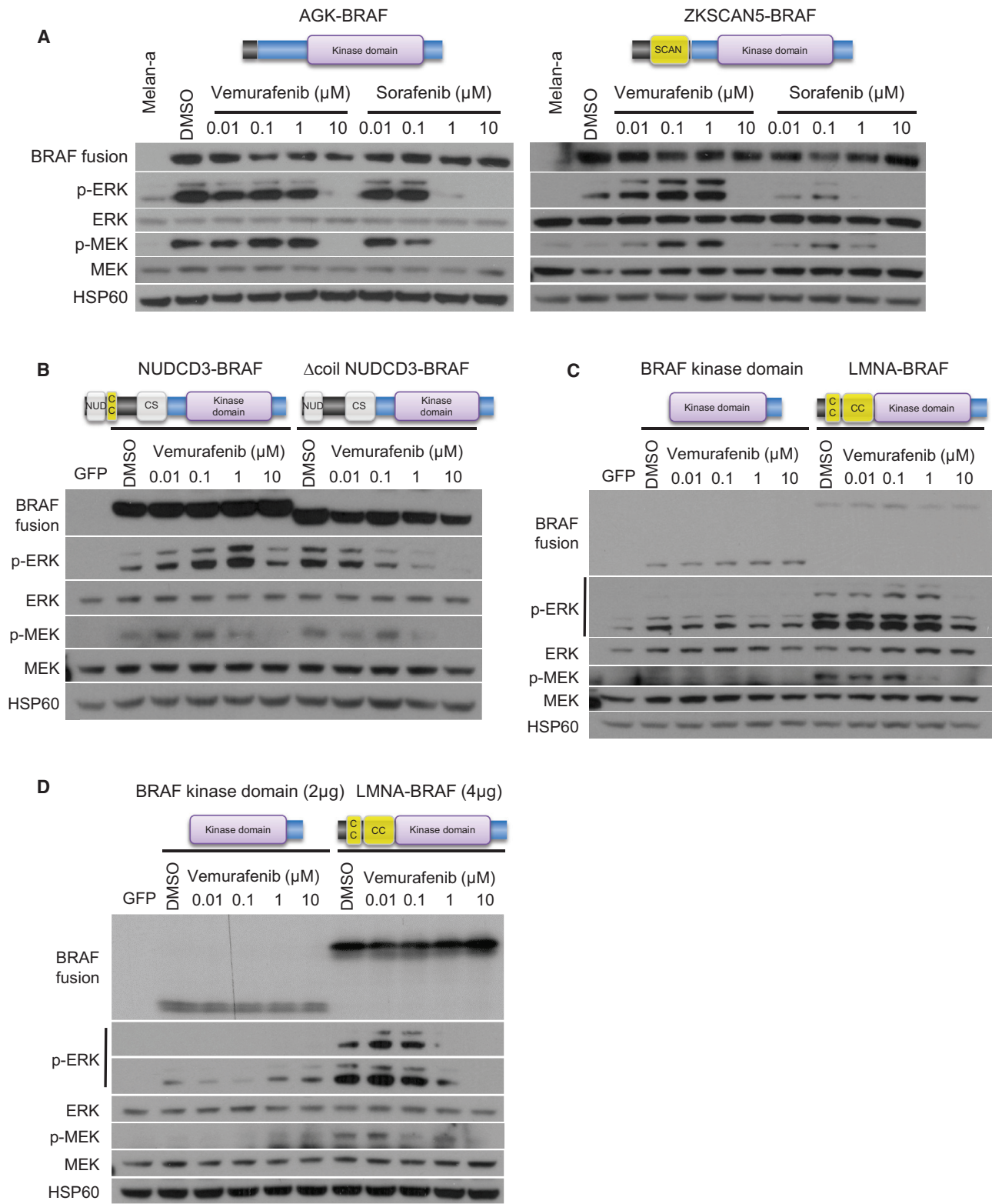
(A) Absolute IC_{50} values of RAF and MEK inhibitors in the two melanoma cell lines harboring an identical AGK-BRAF fusion are higher in C022 cells. Error bar \pm SD.

(B) C022 cells express higher levels of AGK-BRAF fusion protein than C0902 and express no wild-type BRAF protein (see also Figure S4).

(C and D) 293FT cells engineered to express increasing levels of AGK-BRAF fusion protein show increasing resistance to the RAF inhibitor sorafenib (C) and the MEK inhibitor selumetinib (D) after 1 h of treatment.

(E and F) C0902 cells in which the expression level of AGK-BRAF kinase fusion is increased by transient transfection become resistant to the RAF inhibitor sorafenib (E) and the MEK inhibitor trametinib (F) compared to control cells.

(G) The M368 cell line, which is the most resistant line to the MEK and RAF inhibitors (Figure 3A), expresses the highest levels of the BRAF fusion kinase.



(legend on next page)

expression of a NUDCD3-BRAF fusion protein from which the coiled-coil domain was removed did not. Similarly, adding the coiled-coil domain of LMNA to the kinase domain of BRAF (Figure 5C) also induced paradoxical activation. Similar results were obtained at higher expression levels of the LMNA-BRAF fusion protein (Figure 5D).

In summary, presence of a dimerization domain encoded by the 5' partner was necessary and sufficient to promote paradoxical activation of the MAPK signaling pathway in response to first- and second-generation RAF inhibitors.

Paradoxical activation of the MAPK signaling pathway is a well-characterized side effect of classical RAF inhibitors in cells with increased levels of RAS-GTP. In these cells, RAF inhibitors can cause paradoxical activation by promoting the recruitment of RAF dimers, often involving CRAF, to the membrane where the conformational change in the drug-bound RAF protomer induces the transactivation of the other protomer when it is not bound to the drug (Karoulia et al., 2017; Poulikakos et al., 2010). Considering that BRAF fusions present a deletion of their RAS-binding domain, we investigated how their paradoxical activation could fit this model and if BRAF fusions might interact with other RAF isoforms. We first performed RAS-GTP pull-downs to measure the levels of active RAS in our panel of cell lines. As illustrated in Figure 6A, cell lines harboring BRAF fusions had RAS-GTP levels on average 20 times lower than the KRAS^{G12A} mutant cell line M418 and about 6 times lower than 293FT cells but slightly more elevated than BRAF^{V600E} mutant cells. Notably, RAS-GTP levels in the C037 and WM3928 cell lines showing RAF inhibitor-mediated paradoxical activation were not higher than in the other cell lines harboring BRAF fusions. To determine the implication of active RAS in this paradoxical activation of BRAF fusions, we stably transduced primary *HRAS*^{-/-};*NRAS*^{-/-};*KRAS*^{lox/lox} mouse embryonic fibroblasts (MEFs) (Drosten et al., 2010) in which KRAS could be removed by induction of the CRE-recombinase by treatment with 4-hydroxytamoxifen (4OHT), with the NUDCD3-BRAF fusion. In MEFs with intact KRAS, vemurafenib resulted in paradoxical activation of the MAPK signaling pathway as expected (Figure 6B, left panel). Upon presence of 4OHT inducing the excision of *KRAS*^{lox/lox} and complete loss of RAS expression, the vemurafenib-induced paradoxical activation persisted (Figure 6B, right panel). The paradoxical activation was thus mainly RAS-independent, and consistently, there was no significant relocation of the BRAF fusions or other RAF kinases at the membrane upon administration of vemurafenib (Figures 6C and S5A).

The KIAA1549-BRAF fusion commonly found in pilocytic astrocytomas was previously shown to signal as dimer similar to wild-type BRAF and non-V600E BRAF mutants (Sievert et al.,

2013; Yao et al., 2015). We extended this observation to additional BRAF fusion proteins by showing that mutating arginine 509 in the RAF dimer interface dramatically decreased their signaling (Figure S5B), confirming that dimerization is required for BRAF fusion proteins to be active. Notably, disruption of the RAF dimer interface of the NUDCD3-BRAF fusion, in which an additional dimerization domain is contributed by the 5' partner, led to a marked reduction of signaling (Figures 6D and S5B). We ruled out an involvement of other RAF isoforms by performing single and double knockdowns of ARAF and CRAF in BRAF fusion cell lines, which had no effect on the MAPK signaling pathway activation level nor drug-mediated paradoxical activation in response to RAF inhibitors (Figure 6E). Notably, similar experiments performed in the C022 cell line missing the wild-type *BRAF* gene indicated that BRAF fusions can signal independently of all RAF isoforms (Figure S5C).

Altogether, our results indicate that the paradoxical activation observed in BRAF fusions with dimerization domain contributed by their 5' partner is mechanistically distinct from the one previously described for other BRAF oncoproteins in that it is independent of RAS and other RAF isoforms.

BRAF Fusion Proteins Are Highly Sensitive to the Next Generation of α C-IN/DFG-OUT RAF Inhibitors *In Vitro* and *In Vivo*

We tested RAF inhibitors of next generation currently in phase I clinical trials, which became available during the course of our study. They act by stabilizing the α C-helix of RAF kinase in the active (IN) position predicted to inhibit dimeric RAF and thereby prevent classical paradoxical activation (Karoulia et al., 2016). Those RAF inhibitors demonstrated potent inhibition of cell viability (Figure 7A) and MAPK signaling (Figures 7B and S6) across all tested cell lines. Noticeably, no hyperproliferation was observed in the cell lines harboring BRAF fusions with extra dimerization domains, despite a modest increase of MAPK signaling at low drug concentrations that was followed by a dramatic inhibition at higher doses. Nevertheless, the M368 cell line with the high expression of the fusion protein remained more resistant than the other tested cell lines. This resistance was overcome by combination treatment of RAF inhibitors of next generation with MEK inhibitors, which showed a synergistic effect (Figures 7C–7E and S7A–S7G).

We used a xenograft model of the most resistant cell line, M368, to assess the effectiveness of combination treatment with trametinib (0.3 mg/kg oral gavage, twice daily [BID]) and LY3009120 (15 mg/kg oral gavage, BID) *in vivo*. Drug treatments had no significant effect on body weight or mice behavior, indicating that they were well tolerated (Figure S7H). While

Figure 5. Dimerization Domains Contributed by the 5' Partner Induce Paradoxical MAPK Pathway Activation by First- and Second-Generation RAF Inhibitors

- (A) Melan-a cells stably expressing an AGK-BRAF fusion that contains no additional dimerization domain show no paradoxical activation in response to RAF inhibition, whereas melan-a cells expressing ZKSCAN5-BRAF fusion containing an additional dimerization domain (yellow box) do show paradoxical activation. (B) A NUDCD3-BRAF fusion with a dimerization domain in the 5' partner induces paradoxical activation but does not when the dimerization domain is removed. (C) The BRAF kinase domain alone shows no paradoxical activation, but adding a LMNA portion with additional dimerization domains results in paradoxical activation in response to RAF inhibitors. (D) The experiment shown in (C) was repeated with transfecting more LMNA-BRAF fusion than BRAF kinase domain to show that the paradoxical activation was not dependent on the expression level of the fusion.

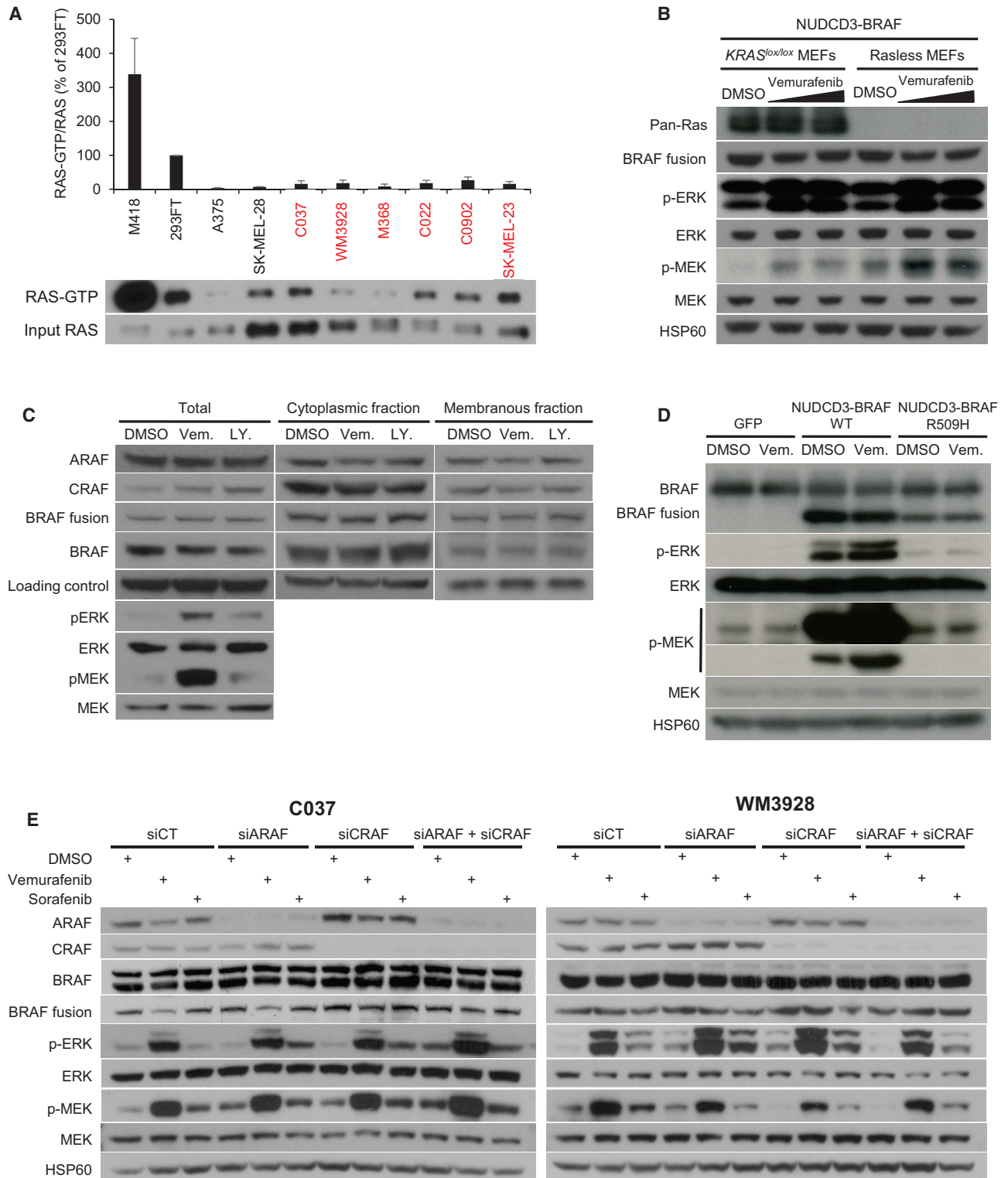


Figure 6. The Paradoxical Activation of BRAF Fusion Kinases Is Independent of RAS and Other RAF Isoforms

(A) The bar graph shows varying levels of RAS-GTP in serum-starved cells with BRAF fusions (red labels), BRAF^{V600E} (A375, SK-MEL-28), or KRAS^{G12A} mutation (M418). RAS-GTP levels shown are the mean \pm SEM of three independent experiments normalized to 293FT cells. Western blots from one representative experiment are shown below.

(legend continued on next page)

monotherapy with trametinib or LY3009120 significantly decreased tumor growth, the combination treatment resulted in a more profound suppression of tumor growth (Figure 7F). Indeed, six out of the eight mice receiving the dual treatment had a stable disease, and the remaining two mice demonstrated a regression of tumor volume of 31% and 44%, respectively, corresponding to a partial response using response evaluation criteria in solid tumors (RECIST) criteria (Figure 7G).

DISCUSSION

Our systematic review of the literature identifies melanocytic tumors with BRAF fusions to be often associated with younger age, histopathological features of spitzoid tumors, and female gender, a criterion not observed in other tumor types with BRAF fusions. While the generation of kinase fusions in papillary thyroid cancer has been associated with the exposure to ionizing radiation (Ricarte-Filho et al., 2013), their occurrence in melanocytic tumors remains to be explained. The young age of the patients, together with the non-specific body distribution of the tumors and their moderate UV signature suggest that BRAF fusions do not originate from UV exposure (Rizzo et al., 2011). Interestingly, we found that 63% of the fusion partners of BRAF reside on the same chromosome 7 and are often associated with complex rearrangements and copy number changes that increase the gene dosage of the fusion gene (Botton et al., 2013). This indicates that they result from multiple simultaneously occurring double stranded DNA breaks of that chromosome, implicating chromothripsis as a likely pathomechanism (Forment et al., 2012). The rearrangements likely result in the disruption of topologically associating domains (TADs) within the DNA sequence and, as a consequence, misregulation of numerous genes (Dixon et al., 2016), which might influence tumor biology and histopathological appearance. Akin to the tandem duplication phenotype of uterine corpus endometrial carcinomas that closely correlates with serous histology (Menghi et al., 2018), disruption of TADs could potentially explain why melanocytic tumors with BRAF fusions have a spitzoid morphology, distinctive from BRAF^{V600E} mutant tumors but similar to tumors driven by other kinase fusions (Wiesner et al., 2014; Yeh et al., 2015, 2016).

Although targeted DNA sequencing is the current gold standard for clinical molecular profiling of tumors (Ross et al., 2016; Zehir et al., 2017), we find that the analysis of RNA is more sensitive in detecting the presence of fusion genes and more accurate in identifying the sequence of the entire fusion kinase including its 5' partner. In our analysis, targeted

sequencing of DNA alone would have missed fusions or misidentified the fusion partner in complex rearrangements. As illustrated in our review of the literature, BRAF fusions of melanocytic tumors show considerably more variation in the combinations with 5' partner genes as compared to other tumor types, which makes it impractical to develop assays for any specific rearrangements. While screening for abnormally sized proteins that reveal the presence of fusion proteins, splice variants (Poulikakos et al., 2011), or kinase domain duplication (Kemper et al., 2016) works well in research settings, RNA analysis appears to be a promising route in development of clinical assays aimed to identify fusion transcripts. Based on the limitations of current assays, it is very likely that the number of patients whose cancers are driven by kinase fusions is currently underestimated.

The sensitivity of melanomas harboring BRAF fusions to immune checkpoint blockade therapies remains to be determined. While a recent study reported good clinical response to immunotherapy in three melanoma patients harboring BRAF fusions (Turner et al., 2019), we reported two patients who progressed (Menzies et al., 2015). It is conceivable that the lower mutation burden of tumors harboring BRAF fusions, as observed in our cell line cohort, might reduce the effectiveness of immune checkpoint blockade compared to low and high cumulative sun-induced damage (CSD) melanomas (Eider et al., 2018) and renders kinase inhibitors a more promising therapeutic approach for the clinical management of tumors harboring such rearrangements. We used unsupervised clustering of viability data from melanoma cell lines harboring BRAF fusions treated with various kinase inhibitors and observed three different response patterns of cells for our *in vitro* experiments. The predictive value of these clusters is limited by the small size of our cohort and will have to be validated on additional cell lines with BRAF fusions as they become available. Nevertheless, our *in vitro* study indicates that vemurafenib and dabrafenib can be counterproductive as therapeutics by inducing paradoxical activation of the MAPK signaling pathway, thereby increasing cell proliferation.

Additional dimerization domains contributed by the 5' partner may stabilize the dimerization of the BRAF fusion protomers, mimicking the interaction that occurs when wild-type RAF binds to GTP-bound RAS dimers (Muratcioglu et al., 2015; Nan et al., 2015). In this scenario, the binding of a classical RAF inhibitor molecule to only one of the two BRAF fusion protomers may trigger transactivation of the other, as previously demonstrated in the case of BRAF/CRAF heterodimers (Hatzivassiliou et al., 2010; Hu et al., 2013; Poulikakos et al., 2010; Röring et al., 2012).

(B) Primary *HRAS*^{-/-}; *NRAS*^{-/-}; *KRAS*^{lox/lox} MEFs stably transduced with the NUDCD3-BRAF fusion that contains a dimerization domain were propagated in the presence of 600 nM 4OHT or vehicle for 3 weeks. Western blot analysis was performed on lysates from serum-starved cells treated for 1 h with 0, 1, or 3 μ M vemurafenib.

(C) Subcellular fractionation of serum-starved C037 cells treated with 1 μ M vemurafenib or 100 nM LY3009120 show no change of cellular location of the BRAF fusion protein under conditions inducing paradoxical activation. HSP60, HSP90, and NRAS were used as loading controls of the total lysate, cytoplasmic and membranous fraction, respectively.

(D) Introduction of the R509H mutation disrupting the RAF dimer interface decreases basal signaling and prevents paradoxical activation of the NUDCD3-BRAF fusions.

(E) Western blots of lysates from serum-starved cell lines with BRAF fusion containing a dimerization domain in their 5' partner silenced for ARAF and/or CRAF, treated or not with 1 μ M RAF inhibitors for 1 h.

See also Figure S5.

As we demonstrated, this deleterious effect can be countered by the use of next-generation RAF inhibitors that bind the kinase domain in a α C-helix-IN/DFG-OUT conformation. These inhibitors differ from prior molecules such as vemurafenib and dabrafenib in that they do not cause negative allosterity that reduces inhibitor binding to the second protomer (Karoulia et al., 2016; Yao et al., 2015). The efficacy of this class of RAF inhibitors to decrease the viability of melanoma cell lines harboring BRAF fusions both *in vitro* and *in vivo* is in agreement with the inhibition of the MAPK signaling pathway observed in an expression model of KIAA1549-BRAF fusion treated with BGB659 (Yao et al., 2015) and fits with the model proposed by Karoulia et al. (2017). Noticeably, despite binding BRAF in its α C-IN/DFG-OUT conformation, sorafenib analogs retain some level of paradoxical activation likely due to their multi-kinase activity that prevents them from effectively inhibiting both BRAF fusion protomers at low drug concentration.

The majority of cell lines with BRAF fusions we tested were less sensitive to the paradox-breaker PLX8394 than cell lines with a BRAF^{V600E} mutation. The results of phase I/II clinical trials with PLX8394 are currently pending, and it remains to be determined whether drug concentrations required to inhibit BRAF fusions can be reached in patients, especially in intra-cranial tumors for which PLX8394 was proposed as a treatment option (Sievert et al., 2013). Moreover, our finding of strong paradoxical activation of the MAPK pathway with increased proliferation in the WM3928 cell line in response to PLX8394 raises caution, as it indicates that the drug might not be universally active against tumors with BRAF fusions. One possible explanation for this phenotype is that PLX8394, originally selected for its ability to prevent BRAF/CRAF heterodimer formation in the context of mutant or GTP-bound RAS (Zhang et al., 2015), is not able to disrupt homo-dimerization of BRAF fusion kinases that are stabilized by an additional dimerization domain encoded by the 5' partner. This hypothesis is supported by results obtained in cells expressing QKI-RAF1 or SRGAP3-RAF1 fusions, which both have such additional dimerization domains contributed by their 5' partner genes (Jain et al., 2017).

KIAA1549 is a highly recurrent fusion partner of BRAF in low-grade astrocytomas. Its structure remains poorly described but the fact that the KIAA1549-BRAF fusions undergo strong paradoxical activation *in vitro* in response to the vemurafenib analog PLX4720 (Sievert et al., 2013) and that sorafenib promotes acceleration of tumor growth in low-grade astrocytoma patients (Karajannis et al., 2014) suggest that it contains a dimerization domain and may benefit from the use of next-generation RAF inhibitors as suggested by Sun et al. (2017). Noticeably,

KIAA1549-BRAF fusions are also found in various other malignancies including melanoma, spindle cell neoplasms, sarcomas, breast carcinoma, and thyroid and lung cancer. It is thus anticipated that their clinical response might be influenced by tissue-specific expression level of the fusion and drug bioavailability at the tumor site.

In summary, this study depicts the clinical features associated with melanocytic tumors harboring BRAF fusions and highlights the diversity of oncogenic rearrangements. Our preclinical *in vitro* and *in vivo* data using tumor cell lines with different endogenous BRAF fusions indicates that a combination of MEK and the next-generation of α C-IN/DFG-OUT RAF inhibitors represents a rational therapeutic approach. Our work demonstrates an underappreciated contribution of the 5' partner gene whose expression level and functional domains markedly influence drug response and possibly biologic behavior.

STAR★METHODS

Detailed methods are provided in the online version of this paper and include the following:

- KEY RESOURCES TABLE
- LEAD CONTACT AND MATERIALS AVAILABILITY
- EXPERIMENTAL MODEL AND SUBJECT DETAILS
 - Clinical cases of BRAF fusion driven tumors
 - Cell lines
 - Mice
- METHOD DETAILS
 - Targeted DNA sequencing
 - RNA sequencing
 - NanoString Assay for AGK-BRAF fusions
 - Western blotting
 - Drugs and reagents
 - Cell proliferation
 - Plasmids
 - Transient transfection of plasmids and siRNAs
 - Stably transduced cells
 - Active RAS pull-down assay
 - Synergy analysis of drug combinations
 - Xenograft experiment
- QUANTIFICATION AND STATISTICAL ANALYSIS
 - Gender Distribution
 - Hierarchical analysis
 - Western blot quantification
 - Isobologram and synergy scores
- DATA AND CODE AVAILABILITY

Figure 7. α C-IN/DFG-OUT RAF Inhibitors Suppress Paradoxical Activation and Synergize with MEK Inhibitors *In Vitro* and *In Vivo*

(A and B) Treatment with α C-IN/DFG-OUT RAF inhibitors compared to DMSO shows dose-dependent reduction of cell viability (A) and MAPK pathway inhibition (B) throughout all cell lines with BRAF fusions and mutation (see also Figure S6). Viability data represent the average of three independent experiments with at least four technical replicates.

(C and D) Combined treatment with the RAF inhibitor LY3009120 and the MEK inhibitor trametinib (C) inhibits signaling after 1 h of treatment and (D) decreases cell viability after 5 days of treatment of M368 cells, the most therapy-resistant cell line harboring a BRAF fusion.

(E) Isobologram analysis of the cell viability results from (D) reveals synergy between LY3009120 and trametinib.

(F) Anti-tumor growth activities of LY3009120 (15 mg/kg, BID) and/or trametinib (0.3 mg/kg, BID) in an M368 subcutaneous xenograft model. Error bar \pm SEM. * $p < 0.05$, ** $p < 0.01$, and *** $p < 0.005$ (unpaired t test, two-tailed).

(G) Waterfall plot of tumor sizes as percent of baseline after 15 days of treatment by RECIST.

See also Figure S7.

SUPPLEMENTAL INFORMATION

Supplemental Information can be found online at <https://doi.org/10.1016/j.celrep.2019.09.009>.

ACKNOWLEDGMENTS

This research was supported in part by NIH grant P01 CA025874 and the Melanoma Research Alliance Established Investigator Award. The cell line establishment program from the Wistar Institute was supported by The Dr. Miriam and Sheldon G. Adelson Medical Research Foundation. T.B. is a recipient of the Franco-American Exchange Prize from Philippe Foundation, Inc., and of a grant from Fondation ARC pour la Recherche sur le Cancer, France.

AUTHOR CONTRIBUTIONS

T.B. and B.C.B. designed the study. A.G. prepared DNA and RNA sequencing libraries. T.B., E.T., I.Y., and A.H.S. analyzed DNA sequencing data. T.B., E.T., and T.Z. analyzed RNA sequencing data. C.B. assisted with the cloning for Figure 5. T.B. conducted and analyzed all functional experiments. T.B. and V.K.M. conducted the animal experiment. R.L.J., S.R., R.B., A.R., N.K.H., K.M.B., and M.H. provided critical reagents and advice. T.B. and B.C.B. wrote the manuscript. All authors reviewed the manuscript.

DECLARATION OF INTERESTS

The authors declare no competing interests.

Received: September 23, 2017

Revised: July 26, 2019

Accepted: September 4, 2019

Published: October 15, 2019

REFERENCES

- Bennett, D.C., Cooper, P.J., and Hart, I.R. (1987). A line of non-tumorigenic mouse melanocytes, syngeneic with the B16 melanoma and requiring a tumour promoter for growth. *Int. J. Cancer* 39, 414–418.
- Botton, T., Yeh, I., Nelson, T., Vemula, S.S., Sparatta, A., Garrido, M.C., Allegra, M., Rocchi, S., Bahadoran, P., McCalmont, T.H., et al. (2013). Recurrent BRAF kinase fusions in melanocytic tumors offer an opportunity for targeted therapy. *Pigment Cell Melanoma Res.* 26, 845–851.
- Chakraborty, R., Burke, T.M., Hampton, O.A., Zinn, D.J., Lim, K.P.H., Abhyankar, H., Scull, B., Kumar, V., Kakkar, N., Wheeler, D.A., et al. (2016). Alternative genetic mechanisms of BRAF activation in Langerhans cell histiocytosis. *Blood* 128, 2533–2537.
- Chmielecki, J., Hutchinson, K.E., Frampton, G.M., Chalmers, Z.R., Johnson, A., Shi, C., Elvin, J., Ali, S.M., Ross, J.S., Basturk, O., et al. (2014). Comprehensive genomic profiling of pancreatic acinar cell carcinomas identifies recurrent RAF fusions and frequent inactivation of DNA repair genes. *Cancer Discov.* 4, 1398–1405.
- Ciampi, R., Knauf, J.A., Kerler, R., Gandhi, M., Zhu, Z., Nikiforova, M.N., Rabes, H.M., Fagin, J.A., and Nikiforov, Y.E. (2005). Oncogenic AKAP9-BRAF fusion is a novel mechanism of MAPK pathway activation in thyroid cancer. *J. Clin. Invest.* 115, 94–101.
- Cin, H., Meyer, C., Herr, R., Janzarik, W.G., Lambert, S., Jones, D.T.W., Jacob, K., Benner, A., Witt, H., Remke, M., et al. (2011). Oncogenic FAM131B-BRAF fusion resulting from 7q34 deletion comprises an alternative mechanism of MAPK pathway activation in pilocytic astrocytoma. *Acta Neuropathol.* 121, 763–774.
- de Hoon, M.J.L., Imoto, S., Nolan, J., and Miyano, S. (2004). Open source clustering software. *Bioinformatics* 20, 1453–1454.
- Diamond, E.L., Durham, B.H., Haroche, J., Yao, Z., Ma, J., Parikh, S.A., Wang, Z., Choi, J., Kim, E., Cohen-Aubart, F., et al. (2016). Diverse and targetable kinase alterations drive histiocytic neoplasms. *Cancer Discov.* 6, 154–165.
- Dixon, J.R., Gorkin, D.U., and Ren, B. (2016). Chromatin domains: the unit of chromosome organization. *Mol. Cell* 62, 668–680.
- Drosten, M., Dhawahir, A., Sum, E.Y.M., Urošević, J., Lechuga, C.G., Esteban, L.M., Castellano, E., Guerra, C., Santos, E., and Barbacid, M. (2010). Genetic analysis of Ras signalling pathways in cell proliferation, migration and survival. *EMBO J.* 29, 1091–1104.
- Elder, D.E., Massi, D., Scolyer, R.A., and Willemze, R. (2018). WHO Classification of Tumours, 4th Edition (International Agency for Research on Cancer).
- Forment, J.V., Kaidi, A., and Jackson, S.P. (2012). Chromothripsis and cancer: causes and consequences of chromosome shattering. *Nat. Rev. Cancer* 12, 663–670.
- Hatzivassiliou, G., Song, K., Yen, I., Brandhuber, B.J., Anderson, D.J., Alvarado, R., Ludlam, M.J.C., Stokoe, D., Gloor, S.L., Vigers, G., et al. (2010). RAF inhibitors prime wild-type RAF to activate the MAPK pathway and enhance growth. *Nature* 464, 431–435.
- Heckman, K.L., and Pease, L.R. (2007). Gene splicing and mutagenesis by PCR-driven overlap extension. *Nat. Protoc.* 2, 924–932.
- Hu, J., Stites, E.C., Yu, H., Germino, E.A., Meharena, H.S., Stork, P.J.S., Kornev, A.P., Taylor, S.S., and Shaw, A.S. (2013). Allosteric activation of functionally asymmetric RAF kinase dimers. *Cell* 154, 1036–1046.
- Hutchinson, K.E., Lipson, D., Stephens, P.J., Otto, G., Lehmann, B.D., Lyle, P.L., Vnencak-Jones, C.L., Ross, J.S., Pietenpol, J.A., Sosman, J.A., et al. (2013). BRAF fusions define a distinct molecular subset of melanomas with potential sensitivity to MEK inhibition. *Clin. Cancer Res.* 19, 6696–6702.
- Jain, P., Fierst, T.M., Han, H.J., Smith, T.E., Vakili, A., Storm, P.B., Resnick, A.C., and Waanders, A.J. (2017). *CRAF* gene fusions in pediatric low-grade gliomas define a distinct drug response based on dimerization profiles. *Oncogene* 36, 6348–6358.
- Jones, D.T.W., Kocialkowski, S., Liu, L., Pearson, D.M., Bäccklund, L.M., Ichimura, K., and Collins, V.P. (2008). Tandem duplication producing a novel oncogenic BRAF fusion gene defines the majority of pilocytic astrocytomas. *Cancer Res.* 68, 8673–8677.
- Jones, D.T.W., Hutter, B., Jäger, N., Korshunov, A., Kool, M., Warnatz, H.-J., Zichner, T., Lambert, S.R., Ryzhova, M., Quang, D.A.K., et al.; International Cancer Genome Consortium PedBrain Tumor Project (2013). Recurrent somatic alterations of FGFR1 and NTRK2 in pilocytic astrocytoma. *Nat. Genet.* 45, 927–932.
- Ju, Y.S., Kim, J.-I., Kim, S., Hong, D., Park, H., Shin, J.-Y., Lee, S., Lee, W.-C., Kim, S., Yu, S.-B., et al. (2011). Extensive genomic and transcriptional diversity identified through massively parallel DNA and RNA sequencing of eighteen Korean individuals. *Nat. Genet.* 43, 745–752.
- Karajannis, M.A., Legault, G., Fisher, M.J., Milla, S.S., Cohen, K.J., Wisoff, J.H., Harter, D.H., Goldberg, J.D., Hochman, T., Merkelson, A., et al. (2014). Phase II study of sorafenib in children with recurrent or progressive low-grade astrocytomas. *Neuro-oncol.* 16, 1408–1416.
- Karouli, Z., Wu, Y., Ahmed, T.A., Xin, Q., Bollard, J., Krepler, C., Wu, X., Zhang, C., Bollag, G., Herlyn, M., et al. (2016). An integrated model of RAF inhibitor action predicts inhibitor activity against oncogenic BRAF signaling. *Cancer Cell* 30, 485–498.
- Karouli, Z., Gavathiotis, E., and Poulikakos, P.I. (2017). New perspectives for targeting RAF kinase in human cancer. *Nat. Rev. Cancer* 17, 676–691.
- Kemper, K., Krijgsman, O., Cornelissen-Steijger, P., Shahrabadi, A., Weeber, F., Song, J.-Y., Kuilman, T., Vis, D.J., Wessels, L.F., Voest, E.E., et al. (2015). Intra- and inter-tumor heterogeneity in a vemurafenib-resistant melanoma patient and derived xenografts. *EMBO Mol. Med.* 7, 1104–1118.
- Kemper, K., Krijgsman, O., Kong, X., Cornelissen-Steijger, P., Shahrabadi, A., Weeber, F., van der Velden, D.L., Bleijerveld, O.B., Kuilman, T., Kluij, R.J.C., et al. (2016). BRAF(V600E) kinase domain duplication identified in therapy-refractory melanoma patient-derived xenografts. *Cell Rep.* 16, 263–277.
- Kim, D., and Salzberg, S.L. (2011). TopHat-Fusion: an algorithm for discovery of novel fusion transcripts. *Genome Biol.* 12, R72.
- Kim, H.S., Jung, M., Kang, H.N., Kim, H., Park, C.-W., Kim, S.-M., Shin, S.J., Kim, S.H., Kim, S.G., Kim, E.K., et al. (2017). Oncogenic BRAF fusions in

- mucosal melanomas activate the MAPK pathway and are sensitive to MEK/PI3K inhibition or MEK/CDK4/6 inhibition. *Oncogene* 36, 3334–3345.
- Kulkarni, A., Al-Hraishawi, H., Simhadri, S., Hirshfield, K.M., Chen, S., Pine, S., Jeyamohan, C., Sokol, L., Ali, S., Teo, M.L., et al. (2017). *BRAF* fusion as a novel mechanism of acquired resistance to vemurafenib in *BRAF*^{V600E} mutant melanoma. *Clin. Cancer Res.* 23, 5631–5638.
- Langmead, B., and Salzberg, S.L. (2012). Fast gapped-read alignment with Bowtie 2. *Nat. Methods* 9, 357–359.
- Li, H., and Durbin, R. (2009). Fast and accurate short-read alignment with Burrows-Wheeler transform. *Bioinformatics* 25, 1754–1760.
- Li, H., and Durbin, R. (2010). Fast and accurate long-read alignment with Burrows-Wheeler transform. *Bioinformatics* 26, 589–595.
- Lu, H., Villafane, N., Dogruluk, T., Grzeskowiak, C.L., Kong, K., Tsang, Y.H., Zagorodna, O., Pantazi, A., Yang, L., Neill, N.J., et al. (2017). Engineering and functional characterization of fusion genes identifies novel oncogenic drivers of cancer. *Cancer Res.* 77, 3502–3512.
- McKenna, A., Hanna, M., Banks, E., Sivachenko, A., Cibulskis, K., Kernytsky, A., Garimella, K., Altshuler, D., Gabriel, S., Daly, M., and DePristo, M.A. (2010). The Genome Analysis Toolkit: a MapReduce framework for analyzing next-generation DNA sequencing data. *Genome Res.* 20, 1297–1303.
- Menghi, F., Barthel, F.P., Yadav, V., Tang, M., Ji, B., Tang, Z., Carter, G.W., Ruan, Y., Scully, R., Verhaak, R.G.W., et al. (2018). The tandem duplicator phenotype is a prevalent genome-wide cancer configuration driven by distinct gene mutations. *Cancer Cell* 34, 197–210.e5.
- Menzies, A.M., Yeh, I., Botton, T., Bastian, B.C., Scolyer, R.A., and Long, G.V. (2015). Clinical activity of the MEK inhibitor trametinib in metastatic melanoma containing *BRAF* kinase fusion. *Pigment Cell Melanoma Res.* 28, 607–610.
- Moriceau, G., Hugo, W., Hong, A., Shi, H., Kong, X., Yu, C.C., Koya, R.C., Samatar, A.A., Khanlou, N., Braun, J., et al. (2015). Tunable-combinatorial mechanisms of acquired resistance limit the efficacy of *BRAF*/MEK cotargeting but result in melanoma drug addiction. *Cancer Cell* 27, 240–256.
- Muratcioglu, S., Chavan, T.S., Freed, B.C., Jang, H., Khavrutskii, L., Freed, R.N., Dyba, M.A., Stefanisko, K., Tarasov, S.G., Gursoy, A., et al. (2015). GTP-dependent K-Ras dimerization. *Structure* 23, 1325–1335.
- Nan, X., Tamgüney, T.M., Collisson, E.A., Lin, L.-J., Pitt, C., Galeas, J., Lewis, S., Gray, J.W., McCormick, F., and Chu, S. (2015). Ras-GTP dimers activate the mitogen-activated protein kinase (MAPK) pathway. *Proc. Natl. Acad. Sci. USA* 112, 7996–8001.
- Nicorici, D., Satalan, M., Edgren, H., Kangaspeska, S., Murumagi, A., Kallioniemi, O., Virtanen, S., and Kilku, O. (2014). FusionCatcher—a tool for finding somatic fusion genes in paired-end RNA-sequencing data. *bioRxiv*. <https://doi.org/10.1101/011650>.
- Olow, A., Mueller, S., Yang, X., Hashizume, R., Meyerowitz, J., Weiss, W., Resnick, A.C., Waanders, A.J., Stalpers, L.J.A., Berger, M.S., et al. (2016). *BRAF* status in personalizing treatment approaches for pediatric gliomas. *Clin. Cancer Res.* 22, 5312–5321.
- Palanisamy, N., Ateeq, B., Kalyana-Sundaram, S., Pflueger, D., Ramnarayanan, K., Shankar, S., Han, B., Cao, Q., Cao, X., Suleman, K., et al. (2010). Rearrangements of the *RAF* kinase pathway in prostate cancer, gastric cancer and melanoma. *Nat. Med.* 16, 793–798.
- Passeron, T., Lacour, J.-P., Allegra, M., Ségalen, C., Deville, A., Thyss, A., Giaccherio, D., Ortonne, J.-P., Bertolotto, C., Ballotti, R., and Bahadoran, P. (2011). Signalling and chemosensitivity assays in melanoma: is mutated status a prerequisite for targeted therapy? *Exp. Dermatol.* 20, 1030–1032.
- Poulikakos, P.I., Zhang, C., Bollag, G., Shokat, K.M., and Rosen, N. (2010). *RAF* inhibitors transactivate *RAF* dimers and *ERK* signalling in cells with wild-type *BRAF*. *Nature* 464, 427–430.
- Poulikakos, P.I., Persaud, Y., Janakiraman, M., Kong, X., Ng, C., Moriceau, G., Shi, H., Atefi, M., Titz, B., Gabay, M.T., et al. (2011). *RAF* inhibitor resistance is mediated by dimerization of aberrantly spliced *BRAF*(V600E). *Nature* 480, 387–390.
- Ricarte-Filho, J.C., Li, S., Garcia-Rendueles, M.E.R., Montero-Conde, C., Voza, F., Knäuf, J.A., Heguy, A., Viale, A., Bogdanova, T., Thomas, G.A., et al. (2013). Identification of kinase fusion oncogenes in post-Chernobyl radiation-induced thyroid cancers. *J. Clin. Invest.* 123, 4935–4944.
- Rizzo, J.L., Dunn, J., Rees, A., and Rütger, T.M. (2011). No formation of DNA double-strand breaks and no activation of recombination repair with UVA. *J. Invest. Dermatol.* 131, 1139–1148.
- Röring, M., Herr, R., Fiala, G.J., Heilmann, K., Braun, S., Eisenhardt, A.E., Halbach, S., Capper, D., von Deimling, A., Schamel, W.W., et al. (2012). Distinct requirement for an intact dimer interface in wild-type, V600E and kinase-dead B-Raf signalling. *EMBO J.* 31, 2629–2647.
- Ross, J.S., Wang, K., Chmielecki, J., Gay, L., Johnson, A., Chudnovsky, J., Yelensky, R., Lipson, D., Ali, S.M., Elvin, J.A., et al. (2016). The distribution of *BRAF* gene fusions in solid tumors and response to targeted therapy. *Int. J. Cancer* 138, 881–890.
- Saldanha, A.J. (2004). Java Treeview—extensible visualization of microarray data. *Bioinformatics* 20, 3246–3248.
- Sase, H., Nakanishi, Y., Aida, S., Horiguchi-Takei, K., Akiyama, N., Fujii, T., Sakata, K., Mio, T., Aoki, M., and Ishii, N. (2018). Acquired *JHDM1D*-*BRAF* fusion confers resistance to *FGFR* inhibition in *FGFR2*-amplified gastric cancer. *Mol. Cancer Ther.* 17, 2217–2225.
- Scaffidi, P., and Misteli, T. (2008). Lamin A-dependent misregulation of adult stem cells associated with accelerated ageing. *Nat. Cell Biol.* 10, 452–459.
- Schäfer, T., Merkl, J., Klemm, E., Wichmann, H.-E., and Ring, J.; KORA Study Group (2006). The epidemiology of nevi and signs of skin aging in the adult general population: results of the KORA-survey 2000. *J. Invest. Dermatol.* 126, 1490–1496.
- Schrock, A.B., Zhu, V.W., Hsieh, W.-S., Madison, R., Creelan, B., Silberberg, J., Costin, D., Bharné, A., Bonta, I., Bosemani, T., et al. (2018). Receptor tyrosine kinase fusions and *BRAF* kinase fusions are rare but actionable resistance mechanisms to *EGFR* tyrosine kinase inhibitors. *J. Thorac. Oncol.* 13, 1312–1323.
- Selt, F., Hohloch, J., Hielscher, T., Sahm, F., Capper, D., Korshunov, A., Usta, D., Brabetz, S., Ridinger, J., Ecker, J., et al. (2017). Establishment and application of a novel patient-derived KIAA1549:*BRAF*-driven pediatric pilocytic astrocytoma model for preclinical drug testing. *Oncotarget* 8, 11460–11479.
- Shain, A.H., Yeh, I., Kovalyshyn, I., Sriharan, A., Talevich, E., Gagnon, A., Dummer, R., North, J., Pincus, L., Ruben, B., et al. (2015). The genetic evolution of melanoma from precursor lesions. *N. Engl. J. Med.* 373, 1926–1936.
- Sievert, A.J., Lang, S.-S., Boucher, K.L., Madsen, P.J., Slaunwhite, E., Choudhari, N., Kellet, M., Storm, P.B., and Resnick, A.C. (2013). Paradoxical activation and *RAF* inhibitor resistance of *BRAF* protein kinase fusions characterizing pediatric astrocytomas. *Proc. Natl. Acad. Sci. USA* 110, 5957–5962.
- Stransky, N., Cerami, E., Schalm, S., Kim, J.L., and Lengauer, C. (2014). The landscape of kinase fusions in cancer. *Nat. Commun.* 5, 4846.
- Subbiah, V., Westin, S.N., Wang, K., Araujo, D., Wang, W.-L., Miller, V.A., Ross, J.S., Stephens, P.J., Palmer, G.A., and Ali, S.M. (2014). Targeted therapy by combined inhibition of the *RAF* and *mTOR* kinases in malignant spindle cell neoplasm harboring the KIAA1549-*BRAF* fusion protein. *J. Hematol. Oncol.* 7, 8.
- Sun, Y., Alberta, J.A., Pilarz, C., Calligaris, D., Chadwick, E.J., Ramkissoon, S.H., Ramkissoon, L.A., Garcia, V.M., Mazzola, E., Goumnerova, L., et al. (2017). A brain-penetrant *RAF* dimer antagonist for the noncanonical *BRAF* oncoprotein of pediatric low-grade astrocytomas. *Neuro-oncol.* 19, 774–785.
- Talevich, E., Shain, A.H., Botton, T., and Bastian, B.C. (2016). CNVkit: genome-wide copy number detection and visualization from targeted DNA sequencing. *PLoS Comput. Biol.* 12, e1004873.
- Thorvaldsdóttir, H., Robinson, J.T., and Mesirov, J.P. (2013). Integrative Genomics Viewer (IGV): high-performance genomics data visualization and exploration. *Brief. Bioinform.* 14, 178–192.
- Tucker, M.A. (2009). Melanoma epidemiology. *Hematol. Oncol. Clin. North Am.* 23, 383–395.
- Turner, J.A., Bemis, J.G.T., Bagby, S.M., Capasso, A., Yacob, B.W., Chimed, T.-S., Gulick, R.V., Lee, H., Tobin, R., Tentler, J.J., et al. (2019). *BRAF* fusions

- identified in melanomas have variable treatment responses and phenotypes. *Oncogene* 38, 1296–1308.
- Wang, K., Li, M., and Hakonarson, H. (2010). ANNOVAR: functional annotation of genetic variants from high-throughput sequencing data. *Nucleic Acids Res.* 38, e164.
- Wang, J., Mullighan, C.G., Easton, J., Roberts, S., Heatley, S.L., Ma, J., Rusch, M.C., Chen, K., Harris, C.C., Ding, L., et al. (2011). CREST maps somatic structural variation in cancer genomes with base-pair resolution. *Nat. Methods* 8, 652–654.
- Wiesner, T., He, J., Yelensky, R., Esteve-Puig, R., Botton, T., Yeh, I., Lipson, D., Otto, G., Brennan, K., Murali, R., et al. (2014). Kinase fusions are frequent in Spitz tumours and spitzoid melanomas. *Nat. Commun.* 5, 3116.
- Yao, Z., Torres, N.M., Tao, A., Gao, Y., Luo, L., Li, Q., de Stanchina, E., Abdel-Wahab, O., Solit, D.B., Poulikakos, P.I., and Rosen, N. (2015). BRAF mutants evade ERK-dependent feedback by different mechanisms that determine their sensitivity to pharmacologic inhibition. *Cancer Cell* 28, 370–383.
- Yeh, I., Botton, T., Talevich, E., Shain, A.H., Sparatta, A.J., de la Fouchardiere, A., Mully, T.W., North, J.P., Garrido, M.C., Gagnon, A., et al. (2015). Activating MET kinase rearrangements in melanoma and Spitz tumours. *Nat. Commun.* 6, 7174.
- Yeh, I., Tee, M.K., Botton, T., Shain, A.H., Sparatta, A.J., Gagnon, A., Vemula, S.S., Garrido, M.C., Nakamaru, K., Isoyama, T., et al. (2016). NTRK3 kinase fusions in Spitz tumours. *J. Pathol.* 240, 282–290.
- Yoshihara, K., Wang, Q., Torres-Garcia, W., Zheng, S., Vegesna, R., Kim, H., and Verhaak, R.G.W. (2015). The landscape and therapeutic relevance of cancer-associated transcript fusions. *Oncogene* 34, 4845–4854.
- Yu, H.A., Suzawa, K., Jordan, E., Zehir, A., Ni, A., Kim, R., Kris, M.G., Hellmann, M.D., Li, B.T., Somwar, R., et al. (2018). Concurrent alterations in EGFR-mutant lung cancers associated with resistance to EGFR kinase inhibitors and characterization of MTOR as a mediator of resistance. *Clin. Cancer Res.* 24, 3108–3118.
- Zehir, A., Benayed, R., Shah, R.H., Syed, A., Middha, S., Kim, H.R., Srinivasan, P., Gao, J., Chakravarty, D., Devlin, S.M., et al. (2017). Mutational landscape of metastatic cancer revealed from prospective clinical sequencing of 10,000 patients. *Nat. Med.* 23, 703–713.
- Zhang, C., Spevak, W., Zhang, Y., Burton, E.A., Ma, Y., Habets, G., Zhang, J., Lin, J., Ewing, T., Matusow, B., et al. (2015). RAF inhibitors that evade paradoxical MAPK pathway activation. *Nature* 526, 583–586.

STAR★METHODS

KEY RESOURCES TABLE

REAGENT or RESOURCE	SOURCE	IDENTIFIER
Antibodies		
anti-CRAF	BD Biosciences	Cat#610151; RRID: AB_397552
anti-ARAF	Cell Signaling Technology	Cat#4432; RRID: AB_330813
anti-β-actin	Cell Signaling Technology	Cat#4970; RRID: AB_2223172
anti-Histone H3	Cell Signaling Technology	Cat#4499; RRID: AB_10544537
anti-HSP90	Cell Signaling Technology	Cat#4874; RRID: AB_2121214
anti-phospho-BRAF ^{S445}	Cell Signaling Technology	Cat#2696; RRID: AB_390721
anti-phospho-ERK1/2 ^{T202/Y204}	Cell Signaling Technology	Cat#9101; RRID: AB_331646
anti-phospho-MEK1/2 ^{S217-221}	Cell Signaling Technology	Cat#9121; RRID: AB_331648
anti-PARP	Cell Signaling Technology	Cat#9542; RRID: AB_2160739
anti-Vimentin	Cell Signaling Technology	Cat#5741; RRID: AB_10695459
anti-BRAF	Santa Cruz Biotechnology	Cat#sc-166; RRID: AB_630938
anti-ERK2	Santa Cruz Biotechnology	Cat#sc-1647; RRID: AB_627547
anti-HSP60	Santa Cruz Biotechnology	Cat#sc-1722; RRID: AB_2233354
anti-MEK1/2	Santa Cruz Biotechnology	Cat#sc-436; RRID: AB_2142929
anti-NRAS	Santa Cruz Biotechnology	Cat#sc-31; RRID: AB_628041
Anti-Pan Ras	Santa Cruz Biotechnology	Cat#sc-166691; RRID: AB_2154229
anti-Goat IgG-HRP	Santa Cruz Biotechnology	Cat#sc-2033; RRID: AB_631729
anti-Mouse IgG-HRP	GE Healthcare Biosciences	Cat# NA931V; RRID: AB_772210
anti-Rabbit IgG-HRP	GE Healthcare Biosciences	Cat# NA934V; RRID: AB_772206
Bacterial and Virus Strains		
One Shot Stbl3 chemically competent <i>E. coli</i>	Thermo Fisher Scientific	Cat#C737303
Chemicals, Peptides, and Recombinant Proteins		
Vemurafenib	Selleckchem	Cat#S1267
Dabrafenib	Selleckchem	Cat#S2807
Sorafenib	Selleckchem	Cat#S7397
Regorafenib	Selleckchem	Cat#S1178
RAF265	Selleckchem	Cat#S2161
Selumetinib	Selleckchem	Cat#S1008
Trametinib	Selleckchem	Cat#S2673
PD0325901	Selleckchem	Cat#S1036
GDC0623	Selleckchem	Cat#S7553
LY3009120	Selleckchem	Cat#S7842
Lifirafenib	Selleckchem	Cat#S7926
CCT196969	Selleckchem	Cat#S7743
MLN2480	Selleckchem	Cat#S7121
4-Hydroxytamoxifen (4OHT)	Sigma-Aldrich	Cat#H6278
Hydroxypropylmethylcellulose	Sigma-Aldrich	Cat#H7509
Tween 80	Sigma-Aldrich	Cat#P4780
Phorbol 12-myristate 13-acetate (TPA)	Sigma-Aldrich	Cat#P8139
Blasticidin S-hydrochloride	Thermo Fisher Scientific	Cat#A1113903
Tween 20	Thermo Fisher Scientific	Cat#BP337500
RIPA Lysis and Extraction Buffer	Thermo Fisher Scientific	Cat#89901
Halt Protease and Phosphatase Inhibitor Cocktail	Thermo Fisher Scientific	Cat#78445

(Continued on next page)

Continued

REAGENT or RESOURCE	SOURCE	IDENTIFIER
Tris Buffered Saline	Santa Cruz Biotechnology	Cat#sc362305
Cycloheximide	Santa Cruz Biotechnology	Cat#sc-3508
Polybrene	Santa Cruz Biotechnology	Cat#sc-134220
Immobilon Forte Western HRP substrate	Merck Millipore	Cat#WBLUF0500
Matrigel® Basement Membrane Matrix High Concentration LDEV-free	Corning	Cat#354248
Non-fat dry milk	Biorad	Cat#1706404
Bovine Serum Albumin fraction V	MilliporeSigma	Cat#2960
PLX8389	Plexxikon	N/A
Critical Commercial Assays		
Subcellular Protein Fractionation Kit for Cultured Cells	Thermo Fisher Scientific	Cat#78840
NuPAGE 4-12% Bis-Tris Protein Gels	Thermo Fisher Scientific	Cat#NP0336BOX
CellTiter 96 Aqueous One Solution Cell Proliferation Assay, 1,000 assays	Promega	Cat#G3580
Active Ras Pull-Down and Detection Kit	Thermo Fisher Scientific	Cat#16117
Pierce BCA Protein Assay Reagent A	Thermo Fisher Scientific	Cat#23228
Pierce BCA Protein Assay Reagent B	Thermo Fisher Scientific	Cat#23224
QIAamp DNA Kit	QIAGEN	Cat#51304
RNeasy kit	QIAGEN	Cat#74104
Ovation Ultralow Library System	Nugen	Cat#0331-32
Nextflex	Bioo Scientific	Cat#5140-53
KAPA Hyper Prep Kit	Roche	Cat#KK8504
Nimblegen SeqCap EZ Choice	Roche	Cat#06588786001
QuikChange Lightning Site-Directed Mutagenesis Kit	Agilent	Cat#210518
NEBNext mRNA Library Prep Reagent Set for Illumina	New England Biolabs	Cat#E6100S
TruSeq RNA Access Library Prep Kit	Illumina	RS-301-2001
Deposited Data		
Targeted DNA and RNA sequencing data	This paper	“SRA: SRP118152”
Frequencies of BRAF fusions detected in cohorts of melanoma patients	N/A	Table S1
Review of 100 cases of melanocytic tumors harboring BRAF fusions	N/A	Table S2
Gender distribution of BRAF fusions cases across tumor types	N/A	Table S3
Experimental Models: Cell Lines		
A375	ATCC	CRL-11619
SK-MEL-28	ATCC	HTB-72
SK-MEL-23	MSKCC cell line collection	N/A
C8161	Gift from Dr. Meenhard Herlyn	N/A
WM3622	Gift from Dr. Meenhard Herlyn	N/A
WM3918	Gift from Dr. Meenhard Herlyn	N/A
WM3928	Gift from Dr. Meenhard Herlyn	N/A
M230	Gift from Dr. Antoni Ribas	N/A
M257	Gift from Dr. Antoni Ribas	N/A
M285	Gift from Dr. Antoni Ribas	N/A
M368	Gift from Dr. Antoni Ribas	N/A
M375	Gift from Dr. Antoni Ribas	N/A
M418	Gift from Dr. Antoni Ribas	N/A
C022	Gift from Dr. Nicholas K. Hayward	N/A

(Continued on next page)

Continued

REAGENT or RESOURCE	SOURCE	IDENTIFIER
C037	Gift from Dr. Nicholas K. Hayward	N/A
C0902	Gift from Dr. Robert Ballotti	N/A
Melan-a	Gift from Dr. Dorothy C Bennett	N/A
HRAS ^{-/-} ;NRAS ^{-/-} ;KRAS ^{lox/lox} mouse embryonic fibroblasts	Gift from Dr. Frank McCormick	N/A
293FT	Thermo Fisher Scientific	Cat#R70007
Experimental Models: Organisms/Strains		
Female athymic homozygous NU/J mice	The Jackson Laboratory	Stock#002019
Oligonucleotides		
SMARTpool siRNA ARAF	Dharmacon	Cat#L-003563-00-0005
SMARTpool siRNA BRAF	Dharmacon	Cat#L-003460-00-0005
SMARTpool siRNA RAF1	Dharmacon	Cat#L-003601-00-0005
Non-targeting pool control siRNA	Dharmacon	Cat#D-001810-10-05
Cloning and sequencing primers	This paper	Table S8
Quikchange primers	This paper	Table S8
NanoString probes	This paper	Table S8
Recombinant DNA		
pENTR/D-TOPO cloning kit	Thermo Fisher Scientific	K240020
pLenti6.3/TO/V5-Dest and packaging vectors	Thermo Fisher Scientific	A11144
pLenti6.3-AGK-BRAF	Botton et al., 2013	N/A
pLenti6.2 GFP	Botton et al., 2013	N/A
pLenti6.2 BRAF ^{V600E}	Botton et al., 2013	N/A
pBABE-puro-GFP-wt-lamin A	Scaffidi and Misteli, 2008	Addgene Plasmid #17662
pBluescriptR-ZKSCAN5	Harvard PlasmID	Plasmid ID HsCD00333692
pCMV-SPORT6-NUDCD3	Harvard PlasmID	Plasmid ID HsCD00324123
pLenti6.3-ZKSCAN5-BRAF	This paper	N/A
pLenti6.3-NUDCD3-BRAF	This paper	N/A
pLenti6.3-Δcoil-NUDCD3-BRAF	This paper	N/A
pLenti6.3-LMNA-BRAF	This paper	N/A
pLenti6.3-BRAF kinase domain	This paper	N/A
pLenti6.2 BRAF ^{V600E/R509H}	This paper	N/A
pLenti6.3-BRAF kinase domain ^{R509H}	This paper	N/A
pLenti6.3-AGK-BRAF ^{R509H}	This paper	N/A
pLenti6.3-NUDCD3-BRAF ^{R509H}	This paper	N/A
Software and Algorithms		
Burrows-Wheeler Aligner (BWA)	Li and Durbin, 2009	http://bio-bwa.sourceforge.net/
Burrows-Wheeler Aligner Smith-Waterman (BWA-SW)	Li and Durbin, 2010	http://bio-bwa.sourceforge.net/
Genome-Analysis Toolkit	McKenna et al., 2010	https://software.broadinstitute.org/gatk/
Picard	https://broadinstitute.github.io/picard/	https://broadinstitute.github.io/picard/picard/
Annovar	Wang et al., 2010	http://annovar.openbioinformatics.org/en/latest/
CNVkit	Talevich et al., 2016	https://cnvkit.readthedocs.io/en/stable/
Clipping REveals STructure (CREST)	Wang et al., 2011	https://www.stjuderresearch.org/site/lab/zhang
Integrated Genomics Viewer (IGV)	Thorvaldsdóttir et al., 2013	http://software.broadinstitute.org/software/igv/
Compute pI/Mw tool	https://web.expasy.org/compute_pi/	https://web.expasy.org/compute_pi/
Bowtie2	Langmead and Salzberg, 2012	http://bowtie-bio.sourceforge.net/bowtie2/

(Continued on next page)

Continued

REAGENT or RESOURCE	SOURCE	IDENTIFIER
FusionCatcher	Nicorici et al., 2014	https://github.com/ndaniel/fusioncatcher
TopHat-Fusion	Kim and Salzberg, 2011	https://ccb.jhu.edu/software/tophat/fusion_index.shtml
Chalice Analyzer online	Horizon Discovery	
Cluster 3.0	de Hoon et al., 2004	http://bonsai.hgc.jp/~mdehoon/software/cluster/software.htm
Java TreeView 1.1.6r4	Saldanha, 2004	http://jtreeview.sourceforge.net/
Image Studio Lite 5.2	LI-COR Biosciences	https://www.licor.com/bio/image-studio-lite/download
Sign and binomial test	Graphpad	https://www.graphpad.com/quickcalcs/binomial1.cfm

LEAD CONTACT AND MATERIALS AVAILABILITY

Further information and requests for resources and reagents should be directed to and will be fulfilled by the Lead Contact, Boris Bastian (Boris.Bastian@ucsf.edu). All plasmids generated in this study will be made available on request but we may require a payment and/or a completed Materials Transfer Agreement if there is potential for commercial application.

EXPERIMENTAL MODEL AND SUBJECT DETAILS**Clinical cases of BRAF fusion driven tumors**

Cases of melanocytic tumors harboring BRAF fusions analyzed in [Figure 1](#) were identified by the systematic review of Pubmed using the key words “BRAF fusion,” “BRAF fusions,” “BRAF rearrangement,” “BRAF rearrangements,” “BRAF translocation” and “BRAF translocations,” and the consultation of articles sequencing series of melanocytic tumors. Detailed description of studied cases is provided in [Table S2](#).

Cell lines

To warrant authentication, all melanoma cell lines were obtained from the ATCC or directly from their institution of origin. The C8161, WM3622, WM3918, WM3928 melanoma lines were gifted by the Herlyn lab (The Wistar Institute, Philadelphia, PA, USA) and maintained in Tu2% growth medium (80% MCDB153, 20% Leibovitz's L-15, 2% FBS, 5 $\mu\text{g ml}^{-1}$ bovine insulin and 1.68 mM CaCl_2). The BRAF^{V600E} mutant melanoma lines A375 (CRL-1619) and SK-MEL-28 (HTB-72) were purchased from ATCC (Manassas, VA, USA). The M230, M257, M285, M368, M375, M418 melanoma lines were gifted by the Ribas lab (University of California, Los Angeles, Los Angeles, CA, USA). The C022 and C037 melanoma lines were gifted by the Hayward lab (QIMR Berghofer Medical Research Institute, Brisbane, QLD, Australia). The C0902 melanoma line was gifted by the Ballotti lab (Université Côte d'Azur, Nice, France). The SK-MEL-23 melanoma line was obtained from the Memorial Sloan Kettering Cancer Center cell line collection (New York, NY, USA). The A375, SK-MEL-28, M230, M257, M285, M368, M375, M418, C022, C037, SK-MEL-23 and C0902 were maintained in glutamine-containing RPMI-1640 supplemented with 10% heat-inactivated fetal bovine serum, penicillin (100 units ml^{-1}) and streptomycin (50 mg ml^{-1}). Melan-a mouse immortalized melanocytes were generously provided by Dr. Dorothy C Bennett (St George's Hospital, University of London, London, UK) and maintained as previously described ([Bennett et al., 1987](#)). The 293FT cells were purchased from Thermo Fisher Scientific (Waltham, MA, USA) and maintained in DME-H21 medium containing 10% heat-inactivated fetal bovine serum, MEM Non-Essential Amino Acids (0.1 mM), sodium pyruvate (1 mM), penicillin (100 units ml^{-1}) and streptomycin (50 mg ml^{-1}). Previously described primary *HRAS*^{-/-}; *NRAS*^{-/-}; *KRAS*^{lox/lox} MEFs ([Drosten et al., 2010](#)) were generously provided by Dr. Frank McCormick (University of California San Francisco, San Francisco, CA, USA). All cells were maintained in humidified incubators at 37°C with 5% CO_2 .

For experimental purpose A375, SK-MEL-28 and the six cell lines harboring BRAF fusions were plated in glutamine-containing RPMI-1640 supplemented with 10% heat-inactivated fetal bovine serum, penicillin (100 units ml^{-1}) and streptomycin (50 mg ml^{-1}). To study signaling, 293FT cells were depleted from serum for 4 hours before collection of cellular lysates. Other cell lines were depleted from serum (and TPA in the case of melan-a cells) for 6 hours before collection of cellular lysates.

Mice

Animal experiment was carried out in accordance with the Declaration of Helsinki and approved by the University of California, San Francisco Institutional Animal Care and Use Committee. Animal sample size was calculated based on previous studies. A total of 4.5 million M368 melanoma cells harboring a BRAF fusion were mixed 1:1 with Matrigel basement membrane high concentration LDEV-free (Corning, Corning, NY, USA) and injected subcutaneously in the right flank of 6-week-old female athymic mice homozygous for

Foxn1nu (The Jackson Laboratory, Bar Harbor, ME, USA). After tumor volume, measured three times a week with a caliper and calculated by the formula $V = (L \times W^2)/2$ reached an average of 120 mm³, mice were randomized into 4 groups. Endpoint was defined as the completing of 15 days of treatment or tumor volume exceeding 1 cm³ or signs of treatment toxicity monitored by behavior and weight (see Figure S7H). Mice were kept in the animal facility with 12 hours of light and dark cycle with food and water *ad libitum*.

METHOD DETAILS

Targeted DNA sequencing

Cell line DNA was extracted using the QIAamp DNA kit (QIAGEN, Germantown, MD, USA) according to the manufacturer's protocol. Multiplex library preparation was performed with the Ovation Ultralow Library System (NuGEN, San Carlos, CA, USA), Nextflex (Bio Scientific, Austin, TX, USA) or Kapa Hyper Prep Kit (Kapa Biosystems, Wilmington, MA, USA) according to the manufacturer's specifications, with up to 200 ng of sample DNA (See Table S7). Hybridization capture of pooled libraries was performed with custom-designed bait libraries (NimblegenSeqCap EZ Choice) spanning ~1.8 Mb of the genome, including the exons of *BRAF*, *NRAS*, *HRAS*, *KIT*, *GNAQ*, and introns 7, 8, 9, and 10 of *BRAF*. The target intervals cover mostly exonic but also some intronic and untranslated regions of 365 (version 1) or 293 (version 2) target genes (See Table S7). The target genes were curated to comprise common cancer genes with particular relevance to melanoma.

Captured libraries were sequenced as paired-end 100-bp reads on a HiSeq 2000 or HiSeq 2500 instrument (Illumina, San Diego, CA, USA). Sequence reads were mapped to the reference human genome (hg19) by use of the Burrows – Wheeler aligner (BWA) (Li and Durbin, 2010). Recalibration of reads and variant calling were performed with the Genome Analysis Toolkit (McKenna et al., 2010). Coverage and sequencing statistics were determined with Picard CalculateHsMetrics and Picard CollectInsertSizeMetrics (<http://broadinstitute.github.io/picard>) (See Table S7). Variant annotation was performed with Annovar (Wang et al., 2010). Copy number variations were inferred with the use of CNVkit version 0.8.5 (Talevich et al., 2016) (<https://github.com/etal/cnvkit>). Allelic imbalance of single-nucleotide polymorphisms was used to call loss of heterozygosity as previously described (Shain et al., 2015). For fusion detection, read pairs with one or more reads unaligned, with insert sizes of > 1000 bp or with soft clipping of at least one read were extracted and realigned by the use of BWA-SW (Li and Durbin, 2010) and used as input to CREST (Wang et al., 2011). Structural variants predicted by CREST were reviewed by visual inspection in the Integrative Genomics Viewer (Thorvaldsdóttir et al., 2013). We predicted the resulting fusion transcripts by joining the exon directly upstream of the genomic breakpoint with the exon directly downstream. Protein sequences were then determined from the predicted transcripts and molecular weight was estimated by the Compute pI/Mw tool from ExpASy. In the absence of matching normal, the number of mutation per megabase was estimated by filtering out common SNPs listed on the 1000 Genomes Project, the Exome Sequencing Project 6500 and a list of sequencing artifacts recurrently detected in normal samples run on our platform from the list of point mutations detected by Annovar on targeted DNA-seq and dividing this number by the footprint of the sequencing library. UV signature was inferred by quantifying the percentage of C > T and G > A transitions in mutated genes as previously filtered.

RNA sequencing

Cell line RNA was extracted using the RNeasy kit (QIAGEN, Germantown, MD, USA) according to the manufacturer's protocol. RNA sequencing of mRNA transcripts from C022 and C037 was performed by the commercial service center Macrogen (Seoul, Korea) as previously described (Ju et al., 2011). RNA sequencing of mRNA transcripts from C0902 was performed by Genewiz, Inc (South Plainfield, NJ, USA). For other lines, double-stranded cDNA was synthesized with the NEBNext mRNA Library Prep Reagent Set for Illumina (New England Biolabs, Ipswich, MA) with up to 250ng of input total RNA. Library preparation was performed with the TruSeq RNA Access Library Prep kit (Illumina, San Diego, CA, USA) according to the manufacturer's protocol. Sequencing was performed on the HiSeq 2500 instrument (Illumina) with paired-end 100-bp reads. Sequence reads were mapped to the reference human genome (hg19) and transcriptome with BOWTIE2 (Langmead and Salzberg, 2012), and fusions were identified by FusionCatcher (Nicorici et al., 2014) or TopHat-Fusion (Kim and Salzberg, 2011) and reviewed by visual inspection in the Integrative Genomics Viewer. Predicted protein sequences were then determined from the detected transcripts.

NanoString Assay for AGK-BRAF fusions

Detection of *AGK-BRAF* fusion transcripts using NanoString nCounter technology (NanoString Technologies, Inc., Seattle, WA) was performed following manufacturer's instructions. In brief, after incubation of total RNA with nCounter probe sets, samples were processed in an automated nCounter Sample Prep Station (NanoString Technologies, Inc., Seattle, WA). nCounter Cartridges (NanoString Technologies, Inc.) containing immobilized and aligned reporter complexes were subsequently imaged on an nCounter Digital Analyzer (NanoString Technologies, Inc.). Reporter counts were collected using NanoString's nSolver analysis software.

Western blotting

Cell lysates were prepared in RIPA buffer supplemented with Halt protease and phosphatase inhibitor cocktail (Thermo Fisher Scientific, Waltham, MA, USA). Equal amounts of protein, as measured by BCA protein assay, were resolved in 4%–12% Bis-Tris NuPage gradient gels (Thermo Fisher Scientific, Waltham, MA, USA) and transferred electrophoretically on a polyvinylidene difluoride membrane with 0.45-micron pore size (Thermo Fisher Scientific, Waltham, MA, USA). Membranes were blocked for 1 h at room

temperature in 5% bovine serum albumin (BSA) or non-fat dry milk in Tris Buffered Saline (Santa Cruz Biotechnology, Dallas, TX, USA) containing 0.1% Tween 20 (Thermo Fisher Scientific, Waltham, MA, USA) (TBST) before being incubated overnight at 4 °C with the primary antibodies. After three washes of 5 min in TBST, secondary antibodies were diluted in 5% non-fat milk in TBST and incubated for 1 h at room temperature. After another three washes in TBST, detection of the signal was achieved by incubating the membrane on Luminata Forte Western HRP substrate (Merck Millipore, Billerica, MA, USA) and exposure on autoradiography films from Denville Scientific (Metuchen, NJ, USA). Films were developed on a Kodak RP X-OMAT M6B series VI B Rapid processor.

The following antibodies were used at the indicated dilution: anti-CRAF (#610151, 1:1000) from BD Biosciences (San Jose, CA, USA); anti-ARAF (#4432, 1:1000), anti- β -actin (#4970, 1:1000), anti-Histone H3 (#4499, 1:1000), anti-HSP90 (#4874, 1:1000), anti-phospho-BRAF (Ser445) (#2696, 1:1000), anti-phospho-ERK1/2 (Thr202/Tyr204) (#9101, 1:1000), anti-phospho-MEK1/2 (Ser217/221) (#9121, 1:1000), anti-PARP (#9542, 1:1000) and anti-Vimentin (#5741, 1:1000) from Cell Signaling Technology (Danvers, MA, USA); anti-BRAF (sc-166, 1:500), anti-ERK2 (sc-1647, 1:2000), anti-HSP60 (sc-1722, 1:6000), anti-MEK (sc-436, 1:1000), anti-NRAS (sc-31, 1:1000) and secondary anti-Goat IgG-HRP (sc-2033, 1:5000) from Santa Cruz Biotechnology (Dallas, TX, USA); secondary anti-Mouse IgG-HRP (NA931V, 1:3000) and secondary anti-Rabbit IgG-HRP (NA934V, 1:3000) from GE Healthcare Biosciences (Piscataway, NJ, USA).

Drugs and reagents

Cycloheximide was purchased from Santa Cruz Biotechnology (Dallas, TX, USA)

Subcellular fractionation was achieved using the Subcellular Protein Fractionation Kit for Cultured Cells according to manufacturer's protocol (Thermo Fisher Scientific, Waltham, MA, USA). Vemurafenib (PLX4032), dabrafenib (GSK2118436), sorafenib (BAY 43-9006), regorafenib (BAY 73-4506), RAF265 (CHIR-265), selumetinib (AZD6244), trametinib (GSK1120212), PD0325901 and GDC0623 were purchased from Selleckchem (Houston, TX, USA). PLX8389 (also called paradox-breaker or PB-3) was generously provided by Plexxikon (Berkeley, CA, USA).

Cell proliferation

Cells were plated in 6-well plates at a density low enough to avoid confluence of the DMSO-treated conditions at the end of the experiment. 24 hours later cells were treated with sorafenib, vemurafenib or regorafenib at 0.03, 0.1, 0.3, 1, 3, 10, 30 μ M; with RAF265 or PLX8394 at 3, 10, 30, 100, 300, 1000, 3000 nM; with dabrafenib at 1, 3, 10, 30, 100, 300, 1000 nM; with selumetinib or PD0325901 at 0.3, 1, 3, 10, 30, 100, 300 nM; with GDC0623 at 0.1, 0.3, 1, 3, 10, 30, 100 nM; or trametinib at 0.01, 0.03, 0.1, 0.3, 1, 3, 10 nM. Five days post-treatment, cells were collected, stained with trypan blue and counted using a TC10 Automated Cell Counter (Bio-Rad Laboratories, Hercules, CA, USA). For the experiments presented in [Figures 7](#) and [S2C](#), cell viability was measured using CellTiter 96 Aqueous One Solution (Promega Corporation, Madison, MI, USA) after five days of treatment according to the manufacturer's instructions.

Plasmids

LMNA (NM_170707.2) cDNA was purchased from Addgene (plasmid# 17662). ZKSCAN5 (NM_014569.3) and NUDCD3 (NM_015332.3) were obtained from Harvard plasmid (HsCD00333692 and HsCD00324123). Fusion constructs were generated by overlap extension PCR ([Heckman and Pease, 2007](#)) using indicated primers. Once PCR products containing the target cDNAs were generated, they were cloned into a pENTR vector using the pENTR/D-TOPO cloning kit (Thermo Fisher Scientific, Waltham, MA, USA). All constructs were subsequently cloned into the pLenti6.3/TO/V5-Dest backbone (Thermo Fisher Scientific, Waltham, MA, USA) and their sequence was entirely verified by Sanger sequencing. The presence of a stop codon at the end of cloned cDNAs prevented the expression of the V5 tag. The pLenti6.3 vector encoding the AGK-BRAF fusion was previously described ([Botton et al., 2013](#)).

The R509H mutation disrupting the RAF dimer interface and the deletion of the coiled-coil domain of the NUDCD3-BRAF fusion were generated using QuikChange Lightning site-directed mutagenesis (Agilent Technologies, Santa Clara, CA, USA).

All primers used are listed in [Table S8](#).

Transient transfection of plasmids and siRNAs

Cells were transfected with plasmid DNA or siRNAs using jetPRIME (Polyplus-transfection, Illkirch, France) according to manufacturer's instructions. ON-TARGETplus human ARAF (L-003563-00-0005), BRAF (L-003460-00-0005), RAF1 (L-003601-00-0005) or control siRNA-SMARTpool were from GE Healthcare Biosciences (Piscataway, NJ, USA). Cells were transfected with 30 nM of the indicated siRNA and assayed 72 hours later.

Stably transduced cells

Lentiviruses were produced by co-transfecting 10 cm plates of 293FT cells with 7 μ g of pLenti6.2-GFP or the construct of interest in a pLenti6.3/TO/V5-Dest backbone together with 9 μ g of packaging vectors. After 24 and 48 hours, filtered supernatants from transfected 293FT cells were applied to melan-a, C0902 or primary *HRAS*^{-/-}; *NRAS*^{-/-}; *KRAS*^{lox/lox} MEFs in the presence of 10 μ g ml⁻¹ of Polybrene (Santa Cruz Biotechnology, Santa Cruz, CA, USA). Cells were selected for at least 20 days using 5 μ g ml⁻¹ of blasticidin S-hydrochloride (Thermo Fisher Scientific, Waltham, MA, USA) after transduction. Primary *HRAS*^{-/-}; *NRAS*^{-/-}; *KRAS*^{lox/lox} MEFs

were then propagated with or without 600 nM of 4OHT for three weeks to fully excise the conditional *KRas*^{lox} alleles and obtain Rasless MEFs.

Active RAS pull-down assay

Cells were cultured in 10 cm dishes until 80%–90% confluence. GTP-bound Ras was quantitated using purified GST-RAF1 Ras-binding domain (RBD) pull-down from detection Kit (Thermo Fisher Scientific,) as instructed by the manufacturers. Since the total RAS expression level varies from one cell line to another, results are presented as the ratio of pull-downed active RAS to total RAS quantified by Image Studio Lite 5.2, normalized as percentage of 293FT cells.

Synergy analysis of drug combinations

M368 cells were plated into 96-well tissue culture plates at 3000 cells per well ($n = 4$ per condition). On the next day, mixtures of inhibitors were added to the cells according to the planned dose matrix. Cell viability was analyzed 5 days later using CellTiter 96 Aqueous One Solution (Promega Corporation, Madison, MI, USA) according to the manufacturer's instructions. Plates were read at 490 nm in a Synergy 2or Epoch plate reader (BioTek, Winooski, VT, USA).

Xenograft experiment

Treatment was performed with LY3009120 15 mg kg⁻¹ and/or trametinib 0.3 mg kg⁻¹ (Selleckchem, Houston, TX, USA) by oral gavage twice daily for 15 days. Inhibitors were dissolved in the vehicle 0.5% hydroxypropylmethylcellulose (Sigma-Aldrich, St. Louis, MO) and 0.2% Tween 80 in distilled water.

QUANTIFICATION AND STATISTICAL ANALYSIS

All quantitative data were collected from experiments performed in at least biological triplicate and expressed as mean \pm SD or SEM as indicated in the figure legend. Differences between groups were assayed with the statistical test indicated in the figure legend using Microsoft Excel or the GraphPad QuickCalcs website <https://www.graphpad.com/quickcalcs/binomial1.cfm> (GraphPad, San Diego, CA). Significant differences were considered when $p \leq 0.05$.

Gender Distribution

In [Figure 1](#), gender distribution was analyzed using two-tail binomial test assuming an expected distribution of 0.5 per gender. This value is knowingly conservative since both benign and malignant melanocytic tumors are more commonly found in patients of male gender ([Schäfer et al., 2006](#); [Tucker, 2009](#)).

Hierarchical analysis

In [Figure 3](#), hierarchical analysis of the results was obtained by complete linkage clustering based on Spearman rank correlation of all data points using Cluster 3.0. Dendrogram was generated with Java TreeView 1.1.6r4.

Western blot quantification

Western blot quantification was performed using Studio Lite 5.2 (LI-COR Biosciences, Lincoln, Nebraska, USA).

Isobologram and synergy scores

In [Figures 7E](#), [S7E](#), and [S7G](#), isobologram analysis and synergy scores were obtained using Chalice Analyzer Online (Horizon Discovery, Cambridge, UK).

DATA AND CODE AVAILABILITY

The accession number for the RNA and DNA sequence data reported in this paper is “SRA: SRP118152.”